

COMMUNITY DETECTION IN WEIGHTED MULTILAYER NETWORKS WITH AMBIENT NOISE

BY MARK HE¹, DYLAN (SHITING) LU², ROSE MARY XAVIER^{2,*} AND JASON XU^{3,†}

¹*Herbert Irving Comprehensive Cancer Center, Columbia University, New York, NY, 11032, USA markhe@live.unc.edu*

²*School of Nursing, University of North Carolina, Chapel Hill, NC, 27599, USA ^{*}rxavier@email.unc.edu (joint senior author)*

³*Statistical Science, Duke University, Durham, NC, 27708, USA [†]jason.q.xu@duke.edu, (joint senior author)*

We introduce a novel model for multilayer weighted networks that accounts for global noise in addition to local signals. The model is similar to a multilayer stochastic blockmodel (SBM), but the key difference is that between-block interactions independent across layers are common for the whole system, which we call *ambient noise*. A single block is also characterized by these fixed ambient parameters to represent members that do not belong anywhere else. This approach allows simultaneous clustering and typologizing of blocks into *signal* or *noise* in order to better understand their roles in the overall system, which is not accounted for by existing Blockmodels. We employ a novel application of hierarchical variational inference to jointly detect and differentiate types of blocks. We call this model for multilayer weighted networks the *Stochastic Block (with) Ambient Noise Model* (SBANM) and develop an associated community detection algorithm. We apply this method to subjects in the Philadelphia Neurodevelopmental Cohort to discover communities of subjects with co-occurrent psychopathologies in relation to psychosis.

1. Introduction

In the advent of more sophisticated data gathering mechanisms and more nuanced conceptions of dependency, relational data have become more widely used than ever before. Statistical network analysis has become a major field of research and is a useful, efficient mode of pattern discovery. Networks representing social interactions, genes, and ecological webs often model members or agents as nodes (vertices) and their interaction as edges. Oftentimes, relational information for the same observations or participants manifest in different modalities, represented by layers. For example, nodes represented by users in a social network such as Twitter can have edges that represent ‘likes’, ‘follows’, and ‘mentions’. In biological networks, modes of interactions such as gene co-expressions or similarities between biotic assemblages may arise among the same sample of study. The study of multilayer networks is especially pertinent in the study of psychiatric data, where distinct diagnoses are not clearly demarcated but rely on constellations of interacting psychopathologies. In this study, we analyze these multimodal psychopathological symptom data using multilayer network analysis.

While network theory for simple graphs is well established [10, 30], the literature concerning weighted, multimodal networks is an emerging field of interest [37, 55]. The field of *community detection* has also grown considerably in recent times [29, 31, 59, 73]. Community detection is an approach used to cluster nodes in a network. Many techniques have been proposed for *unweighted* (binary) graphs including modularity optimization [24, 30], stochastic block models [36, 61, 66, 85], and extraction [44, 89].

Keywords and phrases: Multilayer Network, Community Detection, Stochastic Blockmodel, Variational Inference, High Dimensional Data, Psychosis Spectrum.

The stochastic block model (SBM) is a theoretical model for random graphs [34, 40, 61, 66]; it has also found practical use in community detection [50, 58]. The model lays out a concise formulation for dependency structures within and across communities, but does not model *global* characteristics. Though some methods discern *background* (unclustered) nodes [27, 63, 84], few existing models explicitly account for *community-wise* noise even though it may be useful. We develop a model for multilayer weighted graphs that explicitly accounts for (1) global noise present between differing communities, and (2) dependency structure across layers within communities. We call this model and its associated estimation algorithm as the (multivariate Gaussian) *Stochastic Block (with) Ambient Noise Model* (SBANM).

We develop a novel method that jointly finds clusters in a multilayer weighted network and classifies the *types* of these clusters, namely whether they are (local) signal or (global) noise. We propose a model that discovers and categorizes these communities. We also develop its method of inference, which is additionally useful as many existing multilayer SBM analyses assume known parameters [53, 82]. In the primary case study (Section 5), we use SBANM to find clusters of diagnostic subgroups of patients judged by similarity measures of their psychopathology symptoms.

1.1. Background and Contributions

A canonical example of a globally noisy network is the Erdos-Renyi model where every edge is governed by a single probability. The affiliation model is a weighted extension [4] used to describe a “noisy homogeneous network”; a single *global* parameter θ_{in} dictates the connectivity between all nodes in *any* community, while another θ_{out} controls the connectivity for all nodes in differing communities. A similar model was posited by Arroyo et al. [6] where $\theta_{\text{in}} > \theta_{\text{out}}$ as a baseline for network classification. The weighted SBM and the affiliation model are both *mixture models for random graphs* described by Allman et al. [4, 5].

SBMs were initially used for simple networks [34, 61], but they have been extended to weighted [50] and multilayer settings [6, 64, 76], and in particular time series [52] where clusters across all time points have the same inter-block parameters, but varying between-block interactions. These multilayer SBMs typically do not account for correlations between layers. Some recent studies on binary networks have accounted for correlations across layers [53] and noise [51], but typically assume that parameters are already known.

Though much work has been done on estimating SBMs, not much of it has focused on assessing the *noise* present within them, much less for multilayer weighted graphs. Extraction-based methods identify background nodes to signify lack of community membership [63, 84], but these methods do not attribute any parametric descriptions to these nodes. Some recent work discuss noise in network models that are oftentimes associated with global (i.e. entire-network) uncertainty [13, 51, 60, 87]. However, few have studied *structural noise* that exists between differing communities or that serves as some notion of a residual term (i.e. in regression analysis).

We attempt to address these two gaps in this work. In a multilayer graph with Q ground truth communities (indexed by q), as well as a single block that is considered *noise* (labeled NB for *noise block*), we postulate a model that is *locally unique* with parameter θ_q for all edges within a block indexed at q . The global noise parameter θ_{Noise} describes all interactions between differing blocks as well as NB . A simplified version of this model is presented as follows, but will be written in more detail in Section 3:

$$(1) \quad \theta_{ql} = \begin{cases} \theta_q & \text{if } q = l \text{ and } q \text{ is not } NB \\ \theta_{\text{Noise}} & \text{if } q \neq l \text{ or } q \text{ is } NB \end{cases}.$$

The model combines qualities of the affiliation model [4] with the weighted SBM and extends to multiple layers. Because both the affiliation model and the multilayer SBM are proven to be identifiable by prior work [4, 52], we posit that SBANM is also identifiable. A brief argument is given in Appendix E.1, but deeper investigation remains as future work. One major advantage of a global noise term is its parsimony compared to SBMs. Existing clustering models on multilayer networks, even when accounting for communities that persist across layers [48], still tend toward overparameterization. A reference or *null* group is often used in scientific and clinical settings, an example being the cerebellum in the analysis of brain networks.

1.2. Motivation

We use an example to motivate the proposed model. Suppose there is a social network where nodes represent individuals and weights represent social interactions among them. Individuals naturally interact in cliques where rates of communication are roughly similar (i.e. assortative). Across differing communities, however, rates are assumed to be at a global baseline level. Moreover, interactions among members who are *asocial* and do not belong to any community with a unique signal are similarly modeled as “noise”. Which individuals are still friends with each other after 10 years? Alternatively, how might relationships be broken down – in what ways may work relationships (i.e. co-authorships) correlate with friendships? A schematic figure for this model compared to SBM is presented in Figure 1.

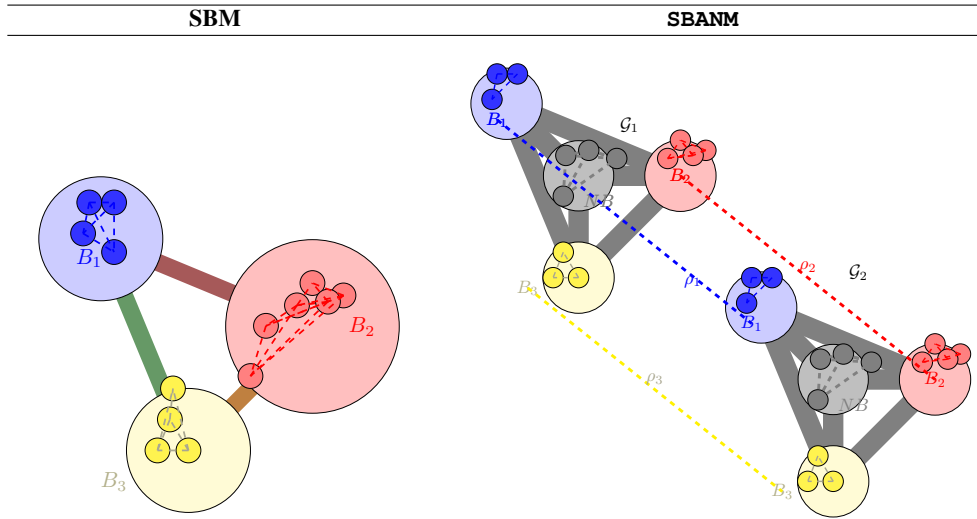


Fig 1: Illustrative example of the types of relationships between blocks for the canonical SBM (left) and SBANM (right). Dashed lines represent the inter-block connectivity among nodes. Large circles represent distinct communities. Solid thick lines represent the inter-community rates of interaction (transition probabilities if binary). In the canonical case (left), the inter-block transitions are all distinct, as denoted by its colors. For the multilayer SBANM case (right), the inter-block parameters are all the same (represented by gray). Ambient Noise (AN) governs the connectivities between blocks and the intra-block connectivity within the block NB across two layers \mathcal{G}_1 and \mathcal{G}_2 with blocks B_1, B_2, B_3 and Noise Block (NB) with correlations ρ_1, ρ_2, ρ_3 across \mathcal{G}_1 and \mathcal{G}_2 .

Psychiatric disorders lack objective measures such as laboratory testing that can confirm or clarify diagnosis. As such, the diagnostic process rests on clinical assessment and is built on codified symptom domains [39]. Psychiatric illnesses, moreover, have multiple causes and

symptoms. There are no laboratory tests for most psychiatric conditions; current diagnostic processes only consider the presence of discrete symptoms and can identify patients who have already have the disease, but it does not help identify who is at risk for the illness in question. One such illness is schizophrenia, a chronic psychotic disorder that affects millions worldwide and imposes a substantial societal burden. Identifying individuals who are at risk for developing this illness is an important issue.

In most existing research on networks, nodes represent individuals and edges are known quantities between nodes. This assumption cannot directly be applied to psychiatric network models to identify communities of individuals with specific conditions, as such relational data are not measurable. They can, however, be estimated from biological and/or psychosocial data, which can then be used for early identification [23, 39, 41]. The flagship criterion that defines the diagnosis of disorders such as schizophrenia is the presence of positive symptoms (DSM-V [8]). This type of categorization is clinically useful but leads to an excess of diagnostic comorbidities and heterogeneities in the clinical presentation of illnesses [23, 41, 81]. More importantly, it is a post-hoc diagnosis: subjects typically are no longer treatable after being diagnosed. With an increase in availability of multimodal data across populations of clinical subjects, community detection is a natural tool for the classification of psychiatric illnesses with multifaceted latent characteristics that could not be directly observed. Moreover, it can pave way for future methods to contribute towards the important objective of early identification.

We use the “co-occurrences” in *psychopathology* symptoms to detect groups of participants with early signs of psychosis. Existing research document “co-occurring and reciprocal relationships between” anxiety, mood, and behavior disorders among cohorts that form a distinct *prodromal* stage that precedes psychosis [25, 43]. We model the *co-occurrence* among common prodromal symptoms as the correlations between networks constructed from anxiety, behavior, and mood disorders. These networks are highly correlated in the prodromal stage, but become independent once the threshold of psychosis is crossed. After the initial episodes of psychosis, the diseases progresses qualitatively out of the *prodrome* and into a psychotic illness. [77]. The *independent* group should manifest high levels of psychosis and represent the group that have transitioned from psychosis prodromal symptoms to active psychotic symptoms [77], while the *correlated* groups of subjects remain in the prodrome.

We hypothesize that the independence assumption of the *NB* cluster from the *SBANM* model corresponds to the decoupled prodromal symptoms in the psychosis symptoms stage. We statistically model the separation in the stages of psychosis symptom onset with the *SBANM* model and algorithm. The model seeks to separate groups that have transitioned to active psychosis symptoms or rather psychosis spectrum from those that have not. We view the correlations between networks constructed from anxiety, behavior, and mood disorders as the analogous to the “co-occurrence and reciprocal relationships” among the prodromal symptoms. Consequently, we interpret clusters with high correlations among these pathologies as indicative of the subjects in varying prodromal stages of psychosis development. In contrast, we hypothesize that the subjects found within *NB*, whose psychopathologies are independent across network layers, are indicative of subjects that have converted to the psychosis spectrum stage. This analysis will be described in more detail in Section 6.

In Section 2, we describe the terminology alongside the *Philadelphia Neurodevelopmental Cohort* (PNC) data for the main case study. We then describe the model and its method of (variational) inference in Section 3, and its specific mechanics in Section 4. In Section 5, we describe the analysis and results for the PNC case study. In Section 6, Model performance is assessed using synthetic experiments that closely match the results derived from the data. While distinguishing psychosis spectrum will be the primary focus of the proposed methodology, it is useful to find latent structure in other types networks. We also demonstrate

the method on (1) US congressional voting data and (2) human mobility (bikeshare) data in Appendices H,I.

2. Data, Notation, and Terminology

For a K -layer **weighted** multigraph with registered n nodes indexed by the set $[n] = \{1, 2, \dots, n\}$, let \mathbf{G} represent the collection of multilayer weighted graphs with K layers: $\mathbf{G} = \{\mathbf{G}^1, \mathbf{G}^2, \dots, \mathbf{G}^K\}$. Similarly, suppose \mathbf{G} contains Q ground truth communities (blocks) indexed by q , but such that a single block is called *noise block* and labeled NB (indexed by q_{NB}). We let $\mathbf{G}_{ij} = (G_{ij}^1, G_{ij}^2, \dots, G_{ij}^K)$ represent the vector of edge-weights between edges (i, j) across all layers $k = 1, 2, \dots, K$. We define a community as $B_q \subset [n]$ to denote the nodes that are contained in a given block indexed by q in \mathbf{G} , and we let \mathbf{G}_q represent the set of all edges contained in block q across all K layers:

$$(2) \quad \mathbf{G}_q = \{\mathbf{G}_{ij}\}_{i,j \in B_q}.$$

Moreover, we call the set of edges across different blocks q, l (where $q \neq l$) *interstitial noise* (IN), and label it as:

$$(3) \quad \mathbf{G}_{IN} = \{\mathbf{G}_{ij}\}_{i \in B_q, j \in B_l}.$$

We fix **one** block indexed as NB as the *noise block*, where all weights in the block follow a $N_K(\boldsymbol{\mu}_{NB}, \boldsymbol{\Sigma}_{NB})$ distribution. This block represents a null region that is devoid of unique signal, but is distributionally governed by the same characteristics as the interstitial relationships between different blocks. We let \mathbf{G}_{NB} represent the set of edges among members in the “noise block”: $\mathbf{G}_{NB} = \{\mathbf{G}_{ij}\}_{i,j \in NB}$. In the following subsection we describe the data as introduced in the prior section in the context of the notation. In Section 3 we describe the assumption that classifies this notion of noise. Multilayer networks can represent multimodal, longitudinal, or *difference* graphs [37, 55]. The data in the *Philadelphia Neurodevelopmental Cohort* (PNC) (described below) is constructed as a multimodal network, while the applications outlined in Appendices H and I are examples of longitudinal graphs. $\mathbf{G} = \{\mathbf{X}, \mathbf{Y}, \mathbf{Z}\}$ represents anxiety, behavior, and mood psychopathology symptom networks processed from the psychopathological questionnaires for a given set of subjects. With respect to the PNC data, each layer represents one of the psychometric evaluation networks for each disorder.

In the introduction we have mentioned that sex differences play a large role in psychosis onset [42, 54, 62, 71]. The prevalent view is that males typically have a peak in the rates of onset between the ages of 21-25, while females have bimodal peaks much later [71]. We subset the PNC data to *early adult* (ages 18-21) males for the statistical analysis to be concordant with the clinical context. The sample size n in this study represents the 764 *early adult* male subjects. Each node represents a subject, and each weighted edge the transformed similarity ratio between two subjects for anxiety, behavior, and mood symptoms.

The Philadelphia Neurodevelopmental Cohort (PNC) is a community sample of youth subjects aged 8-21 years, recruited from the greater Philadelphia area. These subjects underwent a detailed neuropsychiatric evaluation. [15, 16]. A PNC subsample is used as the primary case study. We assume each member of \mathbf{G} are generated from node-clusters whose (Fisher) transformed edges follow blockwise multivariate normal distributions. We use three general categories of disorders to represent each layer:

1. Anxiety (\mathbf{X}): 44 questions (generalized anxiety, social anxiety, separation anxiety, agoraphobia, specific phobia, panic, obsessive compulsive and post traumatic stress disorder)
2. Behavior (\mathbf{Y}): 22 questions (attention deficit hyperactive disorder, oppositional defiant disorder, conduct disorder)

3. Mood (**Z**): 11 questions (depression and mania),

then Fisher-transformed to produce the weighted edge in graph layer. In these following sections these categories will simply be referred to as “anxiety”, “behavior”, and “mood”. More details on pre-processing can be found in Appendix G.1.

We note that NB could in some cases parallel the notion of an *independent residual*, but not always. In case study of PNC data presented in Section 5, NB corresponds to perhaps the “most informative” discovered block. In Section 1.2 we hypothesize that the independence of NB across layers suggests separation of the prodromal co-occurrences. As such, we say that NB is *noise* only insofar as it is independent across layers, paralleling the analogy of the residual in regression analysis, when in practice NB may correspond to the cluster of the most interest.

3. Model and Inference

SBANM supposes that networks across K layers have the same block structure, while transition parameters between blocks are fixed at the same global level. This model allows detection of common latent characteristics across layers, as well as differential sub-characteristics within blocks (represented by multivariate normal distributions). We assume edges are correlated across layers in the block structures of the proposed model.

DEFINITION 1. (*Correlated Blocks*) For a K -layer (Gaussian) weighted multigraph $\mathbf{G} = \{\mathbf{G}^1, \dots, \mathbf{G}^K\}$ where each layer k represents a graph with n registered nodes, let $B_q \subset [n]$ represent a community housing a partition of nodes $\{i\}_{i \in B_q}$, then each weighted edge between any node in block B_q form a multivariate normal distribution with mean K -dimensional vector $\boldsymbol{\mu}_q$ and $K \times K$ -dimensional covariance matrix $\boldsymbol{\Sigma}_q$:

$$\boldsymbol{\Sigma}_q = \begin{pmatrix} \sigma_{q,1}^2 & \rho_q \sigma_{q,1} \sigma_{q,2} \dots \rho_q \sigma_{q,1} \sigma_{q,K} \\ \rho_q \sigma_{q,2} \sigma_{q,1} & \sigma_{q,2}^2 \dots \rho_q \sigma_{q,2} \sigma_{q,K} \\ \dots & \dots & \dots \\ \rho_q \sigma_{q,K} \sigma_{q,1} & \dots & \sigma_{q,K}^2 \end{pmatrix}.$$

If nodes i, j are in the same block, the distribution of their edges follow a multivariate normal distribution

$$\mathbf{G}_{ij} | \{i \in B_q, j \in B_q\} \sim N_K(\boldsymbol{\mu}_q, \boldsymbol{\Sigma}_q).$$

Note that there is a single correlation parameter ρ_q across all layers for a given block B_q . This is a deliberate choice to induce parsimony and interpretability among block relationships across all layers. We assume that the *noise block* has the same characteristics as the *interstitial noise*; both are drawn from the same distribution AN (*ambient noise*). AN is a global noise distribution that governs both IN and NB :

$$\mathbf{G}_{IN} \stackrel{d}{=} \mathbf{G}_{NB} \sim N_K(\boldsymbol{\mu}_{AN}, \boldsymbol{\Sigma}_{AN}).$$

Because NB and IN both represent “baseline” levels of connectivity for the network, we assume that they both have equivalent characteristics as AN . Members of each block B_q interact with other members in the same block at rates that follow multivariate $\boldsymbol{\mu}_q$ with variance $\boldsymbol{\Sigma}_q$, but interact with members in differing groups $l; l \neq q$ at baseline rates $\boldsymbol{\mu}_{IN}$ with variance $\boldsymbol{\Sigma}_{IN}$, i.e. background interactions.

DEFINITION 2. (*Ambient Noise*) Edges in IN between differing blocks and in NB , are characterized by $(\boldsymbol{\mu}_{AN}, \boldsymbol{\Sigma}_{AN})$: $\boldsymbol{\Sigma}_{AN}$ is a $K \times K$ diagonal matrix with diagonal $(\sigma_{AN,1}^2, \dots, \sigma_{AN,K}^2)$ and off-diagonal entries of 0:

$$\mathbf{G}_{ij} | \{i \in B_q, j \in B_l\} \sim N_K(\boldsymbol{\mu}_{AN}, \boldsymbol{\Sigma}_{AN}).$$

For a community $B_q \subset [n]$ representing the nodes that are contained in block q in a weighted multilayer network \mathbf{G} , we let \mathbf{G}_q represent the set of all edges contained in block B_q across all K layers as defined in Equation (2). Conversely, the set of edges across differing B_q, B_l (i.e. interstitial noise), are defined as in Equation (3).

DEFINITION 3. (*Stochastic Block (with) Ambient Noise Model (SBANM)*) A K -layer (Gaussian) weighted multigraph $\mathbf{G} = \{\mathbf{G}^1, \dots, \mathbf{G}^K\}$ with n nodes (with index set $[n]$) and Q communities (blocks) indexed by q with a single block that is considered *noise* labeled NB (indexed by q_{NB}) with disjoint blocks $\{B_1, B_2, \dots, NB, \dots, B_Q\}_{q,q \leq Q}$ is a SBANM if the following conditions are satisfied.

1. Edges \mathbf{G}_{ij} in the same *correlated* block B_q follows conditional distribution $N_K(\boldsymbol{\mu}_q, \boldsymbol{\Sigma}_q)$ given block memberships. Each two edges in the same block are correlated at rate ρ_q , across any 2 layers.
2. Ambient noise AN with $N_K(\boldsymbol{\mu}_{AN}, \boldsymbol{\Sigma}_{AN})$ governs both IN and NB :
 - a) Edges $i \in B_q$ and $j \in B_l$ ($l \neq q$) follow a $N_K(\boldsymbol{\mu}_{AN}, \boldsymbol{\Sigma}_{AN})$ distribution.
 - b) **One** block NB contains members whose edges are generated from a K -dimensional multivariate normal distribution $N_K(\boldsymbol{\mu}_{AN}, \boldsymbol{\Sigma}_{AN})$.

3.1. Connection to Existing Models

The weighted SBM and the affiliation model are both cases of the *mixture models for random graphs* described by Allman et al. [4, 5]. This general class of network models accounts for assortativity (the tendency for nodes who connect to each other at similar intensities to cluster together) and sparsity (when there are much fewer edges than nodes). In addition to VEM-based inference methods [50, 52, 65] that are extensively referenced in Section 1.1, we also note the existing multilayer work in physics [9, 67, 78, 80] and statistics [45, 49, 82].

Some methods for multigraph SBMs are based on spectral decomposition [6, 53, 82]. These methods are typically applied to binary networks and use different sets of methodology or assumptions such as known parameters [53], but are still similar enough to warrant comparison. The notion of *ambient noise* has been studied in some existing methods. Miao et al. [57] and Priebe et al. [68] present another spectral method for the goal of *core identification* and to separate cores (i.e. signal) from periphery (i.e. noise). Zhang et al. detect noise using correlations [88].

One class of these existing methods model edge connectivity of a (potentially multilayer) network as a function of membership vectors \mathbf{Z}_i (for node i), connectivity matrix \mathcal{R}_k at layer k , and the graph Laplacian [6, 51, 53, 70, 82]. Typically, the connectivity rate corresponds to Bernoulli probabilities (for binary networks), but some of these approaches allow for extensions to the weighted cases [6, 56, 82]. Some work has focused on studying the correlations or linear combinations of the eigenvectors of \mathcal{R}_k , but in most of these cases *conditional independence given labels* between layers is assumed [6, 53]. Another class of these multiplex methods is to devise an optimal aggregation scheme to combine multiple layers and then to use single-graph methods on the resultant network [46]. We consider several special cases of SBANM that reduce to existing models.

1. If all ρ_q were zero (ie. diagonal Σ_q ; no correlations amongst communities) and all the within-community signals were the same, then SBANM is a multivariate extension of the models posited by Allman et al. [4] or Arroyo et al. [7].
2. If $K = 1$, SBANM is a special case of the weighted Gaussian SBM as proposed by Mariadassou et al. where all inter-block connectivities are fixed at a single rate [50].
3. Wang et al. ([82]) constrain the connectivity matrix to a diagonal, which would be analogous to SBANM if ambient noise parameter is fixed at zero: $\theta_{AN} := 0$.
4. Arroyo et al. [6] describe the multilayer SBM [36] for binary graphs which “could be easily extended to the weighted cases”. The model assumes *independent* block parameters \mathcal{R}_k across every layer. If there were parameters θ_{AN} such that $\mathcal{R}_{ql,k} := \theta_{AN}$ (for every $q \neq l$), then a special case of SBANM (where each $\rho_q := 0$) would be recovered.

One could conceive of many different other alternative models without some of the assumptions about ambient noise, such as, for example, a noise block that does not require between-block parameters to be the same. Indeed, there can be many nested variations, but we choose this specific model because it is parsimonious, applicable to the primary case study of the *Philadelphia Developmental Cohort*, and can generalize to other potential uses.

3.2. Hierarchical ELBO

We estimate our proposed model using variational inference (VI) which is used to estimate SBM memberships as well as their parameters [50, 64]. VI is an approach to approximate a conditional density of latent variables using optimization [12, 38]. When optimizing the full likelihood is intractable, simpler surrogates of complicated variables are chosen to create a simpler objective function. The Kullback-Liebler (KL) Divergence between this simpler function and the full likelihood are then minimized. For community detection problems, mean-field (MF) approximations of membership allocations often serve as simpler surrogates of latent approximands to simplify the likelihood function into a lower bound (typically known as *evidence lower bound*: ELBO) [2, 50, 73]. Variational inference is often used for community detection [11, 74, 86, 90].

DEFINITION 4. (*Evidence Lower Bound (ELBO)*) For observed data \mathcal{X} with unknown latent membership variables \mathcal{Z} , the evidence lower bound (ELBO) \mathcal{L} is the approximately optimal likelihood that minimizes the KL Divergence between the approximate distribution $R(\mathcal{Z}, \mathbf{C})$ and the posterior frequency $f(\mathcal{Z}, \mathbf{C}|\mathcal{X})$. It is expressed as follows:

$$\mathcal{L} = \mathbb{E}_{R_{hv}(\mathcal{Z})} [\log f(\mathcal{Z}, \mathcal{X}) - \log R_{hv}(\mathcal{Z})]$$

This ELBO is minimized in variational inference problems. Ranganath et al [69] have shown that the *hierarchical ELBO* yields a tighter bound than the ELBO as defined above.

$$\mathcal{L}' = \mathbb{E}_{R(\mathcal{Z}, \mathbf{C})} [\log f(\mathcal{Z}, \mathcal{X})] - \mathbb{E}_{R(\mathcal{Z}, \mathbf{C})} [\log R(\mathcal{Z}, \mathbf{C})] + \mathbb{E}_{R(\mathcal{Z}, \mathbf{C})} [\log S(\mathbf{C}|\mathcal{Z})].$$

An inequality is shown between the “ordinary” ELBO and the Hierarchical ELBO by Ranganath et al. [69] when minimized with parameters Θ (defined in the following section) (details in Appendix A.1)

$$\min_{\Theta} \mathcal{L}' \leq \min_{\Theta} \mathcal{L}.$$

3.3. Variational EM

Variational EM (VEM) is a demonstrably effective method to estimate SBM and more efficient than other approaches (such as MCMC) [50, 61]. Daudin et al. introduced using VEM

for binary SBMs ([26]. Mariadassou et al. used a similar method for weighted graphs [50]. Though it enables efficient inference, MF VI is limited by its assumption of strong factorization and does not capture posterior dependencies between latent variables arising amongst multilayered networks. Hierarchical variational inference (HVI) provides a natural framework for the two-layered latent structure for multilayer networks. A hierarchy is induced in SBANM by the assumption that all but one block are categorized as *signal*, while a single block is designated as noise. HVI augments variational approximations with priors on its parameters: this assumption allows joint clustering of blocks and their signal-noise differentiation.

We use a similar approach to that originally used in Daudin et al. [26]. The latent variable of interest is the membership allocation matrix \mathcal{Z} , which is a $n \times Q$ matrix where each row $\{\mathcal{Z}_i\}_{i \leq n}$ contains $Q - 1$ zeros and a single one that represents membership at that given entry. We introduce indicator \mathbf{C} of length Q whose values C_q are 0 or 1 to determine if a block q is signal or noise NB .

In addition to the latent variables and memberships, model parameters Θ can be partitioned into Θ_{Signal} and Θ_{Noise} in addition to global parameters α, Ψ :

$$(4) \quad \Theta = \{\alpha, \Psi, \Theta_{\text{Noise}}, \Theta_{\text{Signal}}\}.$$

$\Theta_{\text{Signal}} = \{\mu_q, \Sigma_q\}_{q: 1 \leq q \leq Q; B_q \neq NB}$ represents the model parameters that are unique to each block B_q (not including NB), and also there is one index q_{NB} for noise block NB . $\Theta_{\text{Noise}} = \{\mu_{AN}, \Sigma_{AN}\}$ represents the noise parameters that govern both interstitial noise IN and noise block NB . For NB , each correlation between K layers is set at zero.

The estimation procedure minimizes the hierarchical ELBO with respect to the parameters μ, Σ as well as memberships. The first term $\mathbb{E}_{R(\mathcal{Z}, \mathbf{C})} \log f(\mathcal{X}, \mathcal{Z})$ which represents the observed joint densities of \mathcal{X} and \mathcal{Z} is written in Eq. (12). $\mathbb{E}_{R(\mathcal{Z}, \mathbf{C})} [\log R(\mathbf{C}, \mathcal{Z})]$ represents the joint distribution of the two-tiered variational variables and is written as:

$$\mathbb{E}_{R(\mathcal{Z}, \mathbf{C})} [\log R(\mathcal{Z}, \mathbf{C})] = \sum_{i,q} \tau_{iq} \log \tau_{iq} + \sum_q \left(P_q \log P_q + (1 - P_q) \log(1 - P_q) \right).$$

The third term $\mathbb{E}_{R(\mathcal{Z}, \mathbf{C})} [\log S(\mathbf{C}|\mathcal{Z})]$ described by Ranganath et al. as the ‘recursive variational approximation’ [69] for $R(\cdot)$, is

$$\mathbb{E}_{R(\mathcal{Z}, \mathbf{C})} \log S(\mathbf{C}|\mathcal{Z}) = \sum_{i,q} \left(P_q \log \Psi + (1 - P_q) \log(1 - \Psi) \right) \tau_{iq}.$$

Combining the above terms, the hierarchical ELBO is written as:

$$\begin{aligned} \mathcal{L}' = & \mathbb{E}_{R(\mathcal{Z}, \mathbf{C})} [\log f(\mathcal{X}|\mathcal{Z})] + \sum_{i,q} \left(\tau_{iq} \log \alpha_q + \tau_{iq} \log \tau_{iq} + \left(P_q \log \Psi + (1 - P_q) \log(1 - \Psi) \right) \tau_{iq} \right) \\ & + \sum_q \left(P_q \log P_q + (1 - P_q) \log(1 - P_q) \right). \end{aligned}$$

In the following section we outline the EM framework and then discuss the derivations of $S(\mathbf{C}|\mathbf{Z})$ and $R(\mathbf{Z}, \mathbf{C})$. Detailed derivations for all of these terms can be found in Appendix A.

The main innovation in our approach is in modeling joint approximate conditional distributions of \mathbf{Z} and \mathbf{C} in addition to \mathbf{Z} :

$$(5) \quad R_{\mathcal{X}}(\mathbf{Z}, \mathbf{C}) \approx \prod_{i,q} \left(m(\mathbf{Z}_i, \tau_i) \times \text{Bern}(C_q, P_q) \right).$$

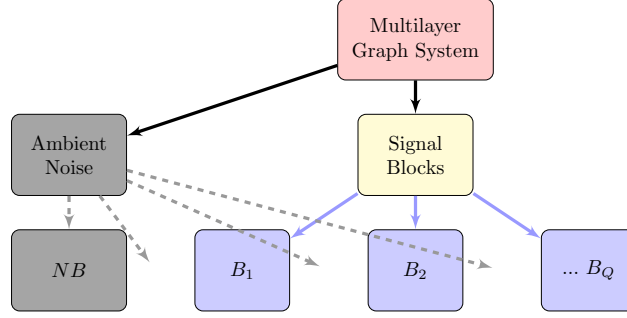


Fig 2: Schematic diagram for the hierarchy of organization for blockstructures with signal/noise differentiation for blocks as the top layer and the actual blocks as the bottom layer.

In Eq. (5) $R_{\mathcal{X}}(\mathcal{Z}, \mathbf{C})$ represents the joint variational distribution of the memberships \mathcal{Z}, \mathbf{C} . The exact joint distribution is unknown, but the hierarchical mean field (MF) approximation $R(\mathcal{Z}, \mathbf{C})$ can be used to obtain a factorized estimate for its marginals [69]. We write the approximate composition of marginals using “ \times ”; $m(\cdot)$ represents the multinomial distribution. The variational approximations of membership matrix \mathcal{Z} is a $n \times Q$ -dimensional matrix τ , each row represents the vector of probabilities that approximates \mathcal{Z}_i [50].

The variational approximation of the indicator C_q at block q is the probability P_q , which typologizes τ . Under variational distribution R , each member i of a block B_q adheres to multinomial distribution with parameter $\tau_{iq} = \mathbb{E}[Z_{iq}]$. P_q is the probability of C_q akin to τ_{iq} . $\Psi := 1/Q$ is the *prior* probability of block $\{B_q\}_{q:q \leq Q}$ to be noise block NB . A derivation for Ψ is given in Appendix C.5.

The hierarchical MF distribution $R_{\text{hv}}(\mathcal{Z})$ as introduced by Ranganath et al. [69] “marginalizes out” the MF parameters in $R_{\mathcal{X}}(\mathcal{Z}, \mathbf{C})$ and is written as

$$R_{\text{hv}}(\mathcal{Z}) = \int R_{\mathcal{X}}(\mathcal{Z}, \mathbf{C}) d\mathbf{C}.$$

Following the methods of estimation proposed in prior work on SBM estimation [26, 50, 65], $R_{\mathcal{X}}(\mathcal{Z}, \tau)$ represents the multinomial variational distribution wherein each τ_{iq} approximates the membership allocations. $R_{\text{hv}}(\mathcal{Z})$ is the same as the variational distribution R in prior work. Prior VEM-based estimation methods focus on optimizing ELBO [26, 50, 64, 65].

\mathcal{L} can be rewritten as the following

$$\mathcal{L} = \mathbb{E}_{R_{\text{hv}}(\mathcal{Z})} [\log f(\mathbf{Z}, \mathbf{X})] + \mathcal{H}_{\text{hv}}(R(\mathcal{Z})),$$

where \mathcal{H} is the entropy of variational variable \mathcal{Z} [69]. A sharper bound than the ELBO is derived by introducing the marginal recursive variational approximation $S(\mathbf{C}|\mathcal{Z})$, and then exploiting the following inequality with joint MF distribution $R(\mathcal{Z}, \mathbf{C})$ and the (hierarchical) entropy $\mathcal{H}(\mathcal{Z})$:

$$(6) \quad \mathcal{H}_{\text{hv}}(R(\mathcal{Z})) \geq -\mathbb{E}_{R(\mathcal{Z}, \mathbf{C})} [\log R(\mathcal{Z}, \mathbf{C})] + \mathbb{E}_{R(\mathcal{Z}, \mathbf{C})} [\log S(\mathbf{C}|\mathcal{Z})].$$

The jointly factorized mean field components are $R(\mathbf{C})$ and $R(\mathcal{Z}|\mathbf{C})$. $R(\mathbf{C})$ is expressed as $R(\mathbf{C}) = \prod_q P_q^{C_q} (1 - P_q)^{1-C_q}$ and $R(\mathcal{Z}|\mathbf{C})$ is written similarly to prior variational mem-

bership variables [26, 50], exponentiated by C_q :

$$R(\mathcal{Z}|\mathbf{C}) = \prod_q \left(\prod_i \tau_{iq}^{Z_{iq}} \right)^{C_q} \left(\prod_i \tau_{iq}^{Z_{iq}} \right)^{1-C_q},$$

combining to form $R(\mathcal{Z}, \mathbf{C}) = R(\mathcal{Z}|\mathbf{C})R(\mathbf{C})$. Moreover, the recursive variational approximation $S(\mathbf{C}|\mathcal{Z})$ [69] estimates the higher-order memberships \mathbf{C} using the basal memberships \mathcal{Z} :

$$S(\mathbf{C}|\mathcal{Z}) = \prod_q \prod_i \left(\Psi^{C_q} (1 - \Psi)^{1-C_q} \right)^{Z_{iq}}.$$

4. Estimation Algorithm

We summarize the targets of inference here to set up the language for the rest of the section. Variational parameters τ_q and P_q (for $q : q \leq Q$) approximate the membership allocations, while model parameters describe the parametric qualities of the blocks. Within the set of model parameters, we further distinguish *local* and *global* parameters. *Local* block-wise parameters are represented by Θ_q , and membership probabilities α_q for each q . *Global* parameters are $\Psi, \Theta_{\text{Noise}}$. We use VEM to estimate variational parameters in the E-step and model parameters in the M-step, alternating these steps until the differences in τ become miniscule. We present the closed-form solutions to all the estimates below, but detailed derivations for every term is found in Appendix C. Operationally, the E-step and M-step are implemented in an alternating fashion until the membership variables τ converge.

First we introduce some more terms

$$(7) \quad f(G_{ij}^k, \mu_q, \Sigma_q) = \frac{1}{2} (G_{ij}^k - \mu_q)^T \Sigma_q^{-1} (G_{ij}^k - \mu_q) - (2\pi)^{K/2} (\log |\Sigma_q|)^{1/2}$$

$$(8) \quad f(G_{ij}^k, \mu_{AN}, \Sigma_{AN}) = \frac{1}{2} (G_{ij}^k - \mu_{AN})^T \Sigma_{AN}^{-1} (G_{ij}^k - \mu_{AN}) - (2\pi)^{K/2} (\log |\Sigma_{AN}|)^{1/2}.$$

Equation (7) denotes the density for edges in a signal block (μ_q, Σ_q) at layer k ; equation (8) denotes density for edges with noise (μ_{AN}, Σ_{AN}) . Graph \mathbf{G} with K graph-layers $\{\mathbf{G}^1, \dots, \mathbf{G}^K\}$, has conditional density

$$(9) \quad \log f(\mathbf{G}|\mathcal{Z}) = \sum_{q: B_q \neq NB} \sum_{q \leq Q} \sum_{k \leq K} \sum_{i, j \leq n} Z_{iq} Z_{jq} f(G_{ij}^k, \mu_q, \Sigma_q) + \\ \mathbf{1}(B_q = NB) \sum_{i, j \leq n} Z_{iq} Z_{jq} f(G_{ij}^k, \mu_{AN}, \Sigma_{AN}) + \sum_{q, l \leq Q: q \neq l} \sum_{i, j \leq n} Z_{iq} Z_{jl} f(G_{ij}^k, \mu_{AN}, \Sigma_{AN}).$$

The log likelihood portion of the ELBO, $\log(f(\mathbf{G}|\mathcal{Z}))$, written above in Equation (9) is comprised of three parts: unique signals for every q (top), the noise block NB (bottom left), and the interstitial noise IN (bottom right). AN is the global *ambient noise* whose parameters govern the *interstitial noise* as well as *noise block* as in Definition 2. Given variational variables τ, \mathbf{P} , the expected likelihood is

$$\mathbb{E}_{R_G}[\log(f(\mathbf{G}|\mathcal{Z}))] = \sum_{q: q \leq Q} \mathbb{P}(B_q \neq NB) \tau_{iq} \tau_{jl} f(G_{ij}^k, \mu_q, \Sigma_q) \\ + \mathbb{P}(B_q = NB) \sum_{i, j: i \neq j} \tau_{iq} \tau_{jl} f(G_{ij}^k, \mu_{AN}, \Sigma_{AN}) + \sum_{q, l \leq Q: q \neq l} \sum_{i, j \leq n} \tau_{iq} \tau_{jl} f(G_{ij}^k, \mu_{AN}, \Sigma_{AN}).$$

The $\mathbb{E}_{R(\mathcal{Z}, \mathbf{C})}[\log f(\mathcal{Z})]$ term restores to the same form as earlier work on SBMs [26, 50]:

$$(10) \quad \mathbb{E}_{R(\mathcal{Z}, \mathbf{C})}[\log f(\mathcal{Z})] = \sum_{i,q} \tau_{iq} \log \alpha_q,$$

where as in prior work [26, 50], the variables α_q represent the membership probabilities of Z_{iq} and sum to 1:

$$(11) \quad \alpha_q = \mathbb{P}(i \in B_q) = \mathbb{P}(Z_{iq} = 1).$$

For the rest of the manuscript we use $\sum_{i,q}(\cdot)$ to signify the double summation across all $i \leq n$ and $q \leq Q$. The expected log frequency of the membership vectors \mathcal{Z} reduces to that in canonical SBMs. Details of this identity are found in Appendix A.2. The joint density is written as:

$$(12) \quad \mathbb{E}_{R(\mathcal{Z}, \mathbf{C})}[\log f(\mathbf{G}, \mathcal{Z})] = \mathbb{E}_{R_G}[\log f(\mathbf{G}|\mathcal{Z})] + \sum_{i,q} \tau_{iq} \log \alpha_q.$$

The expression is written in full in Appendix B.1.

4.1. E-Step

The E-Step of the algorithm estimates the variational variables which represent block memberships Z_{iq} of the nodes i as well as C_q which represent the “memberships of memberships”. First we describe the estimation procedure for the variational approximations τ_{iq} , next we describe the estimation of signal-noise differentiation probabilities P_q . This two-step procedure differs from prior work because of an additional hierarchical estimation step of the higher-level variational variables P_q .

τ_{iq} is estimated by an iterative fixed-point approach. Derivatives for each τ_{iq} are calculated based on model parameters and τ_{jl} ,

$$\begin{aligned} \log(\tau_{iq}) \propto \log(\alpha_q) + \sum_{k \leq K} \sum_{j \leq n} \tau_{jl} & \left(P_q f(G_{ij}^k, \boldsymbol{\mu}_q, \boldsymbol{\Sigma}_q) + (1 - P_q) f(X_{ij}^k, \boldsymbol{\mu}_{AN}, \boldsymbol{\Sigma}_{AN}) \right. \\ & \left. + \sum_{l \leq Q; l \neq q} f(G_{ij}^k, \boldsymbol{\mu}_{AN}, \boldsymbol{\Sigma}_{AN}) \right) - 1 + P_q \log \Psi + (1 - P_q) \log(1 - \Psi). \end{aligned}$$

After exponentiating, the fixed-point equation can feasibly be solved after the iterating the system until relative stability. This is the same approach as most existing literature [26, 50]. P_q are calculated as follows:

$$(13) \quad \widehat{P}_q = 1 - \left(1 + \left[\exp \left(\sum_{k \leq K} \sum_{i,j \leq n} \tau_{iq} \tau_{jq} \left(f(G_{ij}^k, \boldsymbol{\mu}_q, \boldsymbol{\Sigma}_q) - f(G_{ij}^k, \boldsymbol{\mu}_{AN}, \boldsymbol{\Sigma}_{AN}) \right) + \log \left(\frac{1 - \Psi}{\Psi} \right) \right) \right]^{-1} \right)^{-1}.$$

Calculations for each of these terms are provided in Appendices C.1 and C.2. We apply stochastic variational inference (SVI) to calculate the membership parameters τ_{iq} and P_q . Details for SVI are described in Appendix D.1.

4.2. M-Step

Similar to its estimation in Daudin et al. [26], α_q are estimated as follows using Lagrangian multipliers: $\hat{\alpha}_q = \sum_{i,q} \tau_{iq} / n$. The closed-form estimate for the *local* parameters for the mean

vector μ_q for each block q from the M-step is

$$\hat{\mu}_q = \frac{\sum_{i,j} \tau_{iq} \tau_{jq} \mathbf{G}_{ij}}{\sum_{i,j} \tau_{iq} \tau_{jq}} P_q + \mu_{AN} (1 - P_q).$$

In the above, and all subsequent expressions in this subsection, the derivations are located in Appendix C.3. Similarly to mean calculations, the variance calculations (along diagonals) are

$$\hat{\Sigma}_q = \frac{\sum_{i,j} \tau_{iq} \tau_{jq} (\mathbf{G}_{ij} - \mu_q)^2}{\sum_{i,j} \tau_{iq} \tau_{jq}} P_q + \Sigma_{AN} (1 - P_q).$$

The cross-term for two layers h, k is written as:

$$\hat{\Sigma}_{hk,q} = \frac{\sum_{i,j} \tau_{iq} \tau_{jq} (G_{ij}^k - \mu_{q,k})(G_{ij}^h - \mu_{q,h})}{\sum_{i,j} \tau_{iq} \tau_{jq}} P_q.$$

The element-wise correlations at iteration t across layers h, k ($h \neq k$) are then calculated, and the maximum (if $K > 2$) of these values is taken as the putative correlation (across all layers) for block q

$$\hat{\rho}_q = \max_{h,k} \frac{\hat{\Sigma}_{hk,q}^q}{\sqrt{\hat{\Sigma}_q^h \hat{\Sigma}_q^k}}.$$

If $K = 2$ then no maximum needs to be taken. This is an operational step of the optimization and does not necessarily yield closed-form estimates. This value is also known as the *mutual coherence* of estimated correlation matrix and serves as a summary statistic of the estimates for correlations [79].

4.2.1. Estimation of Global Parameters

At each iteration of VEM, the closed-form solutions of the global parameters $\hat{\mu}_{AN}$ and $\hat{\Sigma}_{AN}$ are written as follows. $\hat{\mu}_{AN}$ is

$$(14) \quad \hat{\mu}_{AN} = \Psi \frac{\sum_{j,i} \sum_{l,q:q \neq l} \tau_{iq} \tau_{jl} \mathbf{G}_{ij}}{\sum_{j,i} \sum_{l,q:q \neq l} \tau_{iq} \tau_{jl}} + (1 - \Psi) \frac{\sum_{j,i} \sum_q \tau_{iq} \tau_{jq} (1 - P_q) \mathbf{G}_{ij}}{\sum_{j,i} \sum_q \tau_{iq} \tau_{jq} (1 - P_q)}.$$

The variance of global parameters is similarly calculated as:

$$\hat{\Sigma}_{AN} = \Psi \frac{\sum_{j,i} \sum_{l,q:q \neq l} \tau_{iq} \tau_{jl} (\mathbf{G}_{ij} - \mu_{AN})^2}{\sum_{j,i} \sum_{l,q:q \neq l} \tau_{iq} \tau_{jl}} + (1 - \Psi) \frac{\sum_{j,i} \sum_q \tau_{iq} \tau_{jl} (1 - P_q) (\mathbf{G}_{ij} - \mu_{AN})^2}{\sum_{j,i} \sum_q \tau_{iq} \tau_{jl} (1 - P_q)},$$

the covariance term for global noise, as stated earlier, is zero. Derivations for these expressions are in Appendix C.4.

5. Case Study: PNC Psychopathology Networks

We apply SBANM to the PNC data as the primary case study of this paper. We first construct networks from *anxiety*, *behavior*, and *mood* psychopathologies as described in Section 2, then run the algorithm and subsequently cross validate and empirically verify the results with diagnoses data. We use the notation for data outlined in Section 2: \mathbf{X} represents the layer of symptom response networks for anxiety, \mathbf{Y} for behavior, \mathbf{Z} for mood disorders. Correspondingly, we let $(\mu_{\mathbf{X}}, \mu_{\mathbf{Y}}, \mu_{\mathbf{Z}})$ represent the means of the edge-connections for each block representing anxiety, behavior, and mood with corresponding standard deviations $(\sigma_{\mathbf{X}}, \sigma_{\mathbf{Y}}, \sigma_{\mathbf{Z}})$.

Not much prior work has approached the study of psychiatric conditions using subject-networks. We construct networks of individuals as nodes and their similarity as edges. Distinct conditions are represented by different layers as in a multilayer network. The goal of introducing *ambient noise* to psychopathology symptom networks is to identify groups of people who have similar clinical characteristics and facilitating early identification of individuals at high risk of developing the disorder, in this case psychosis spectrum. Existing machine learning studies of psychosis spectrum typically require input from already-diagnosed subjects. These analyses usually use methods such as logistic regression [18]. However, we aim to classify anxiety, mood, and behavior symptoms to identify who is at risk for psychosis *without* the knowledge of which patients have psychosis spectrum.

Unsupervised analysis is useful in early identification in clinical settings, and we leverage the SBANM method to conduct exploratory analysis that will pave way for potential evidence-based intervention schemes. The developmental periods prior to the onset of psychotic disorders are critical targets of early intervention and as such serve appropriate data for experimental hypotheses of ‘exploratory clustering and classification for the purpose of early detection.

5.1. Scientific Hypothesis

We have introduced literature in Section 1.2 that details specific timing for onset of psychosis in early adult subjects [25, 43, 77]. Tandon et al. and Cupo et al. posits a qualitative change in subjects’ psychopathologies as they transition from the prodromal stage into the psychosis stage [25, 77]. Existing research on pre-psychotic psychopathologies note that “psychotic disorders may be due to *nonpsychotic* common mental disorders such as depression and anxiety” [25]. Cupo et al. document that “epidemiological cohorts also demonstrate co-occurring and reciprocal relationships” between these disorders and psychosis. A myriad of interacting psychopathologies, notably anxiety, behavior disorders, depression, mood disorders known as the psychosis *prodrome* are demonstrated to precede the *first episode* of psychosis [21, 25, 43]. After the first episode, however, the diseases progresses out of the *prodrome* and into “full-blown psychotic illness”: several works have described this decoupling, but few have statistically modeled such a transition [72, 77].

We seek to separate the subjects that have transitioned to psychosis from those who did not. We model the *co-occurrence* among common prodromal symptoms as the correlations between the multilayer network \mathbf{G} constructed from anxiety (\mathbf{X}), behavior (\mathbf{Y}), and mood (\mathbf{Z}) disorders (Section 2). Prior work suggest that there is separation among *independent* and *correlated* groups of subjects (in \mathbf{G}) [77]. We hypothesize that since prodromal symptoms are highly correlated [21, 25], and that they are not associated with non-initial symptoms of psychosis [72], the sample that has converted to psychosis from the prodrome [77] will have *independent*, but exhibit *high rates of*, prodromal symptoms.

We have also traced the literature on sex differences among such co-occurrences between common psychopathologies and their relationship with the first episode of psychosis [42, 54, 62, 71]. We restricted the analysis to the early adult sample for this study, and split up the sexes among subjects to examine the potentially differential effects of clustering (Section 2). Li et al. [71] cite several other works in describing the difference in the peaks of rates of psychosis onset between sex [42, 54, 62]. The consensus among literature describe the peaks of onset as between 21-25 for males, and 25-30 with another peak occurring much later in the middle ages for females. Indeed, for the PNC sample to overlap with the range of psychosis onset, the target sample is male early adults aged 18-21. The sample size is thus 764 subjects.

5.2. Clinical Verification

We ran the SBANM algorithm on early adult PNC subjects stratified by sex. We set $Q = 3$ based on the optimal Integrated Composite Likelihood [52], of which a more detailed explanation is provided in Section 6.1. Table 1 shows the average proportions of subjects who met the criteria for clinical diagnoses of anxiety, mood, and behavior disorders, psychosis spectrum as well as those who were typically developing (TD). The columns after block labels and sizes are positive indicators for anxiety, behavior, and mood disorders. Each clinically identified indicator is ‘yes’ or ‘no’ for each subject. Among males, the results remarkably differentiate rates of psychosis between the NB group and the other correlated clusters (Table 1, left). However, similar rates of differentiation are not found among females (Table 1, right). Furthermore, the rates of psychosis in the independent block NB from clinical verification is 54%, while none fall under *typical development* (TD) among males.

The high rates of psychosis spectrum among males in NB coincide with the clusters where anxiety, mood, and behavioral disorders are disjoint support the hypothesis that the *first episode of psychosis* marks a qualitative transition from prodrome to psychosis spectrum. Furthermore, the timing (in early adult) and difference in the distinguishing characteristics among NB blocks between sex also concur with the prior work in timing of psychosis onset. The most significant clustering result is found among subjects in the NB block (Table 1). Among these subjects, their high rates of psychosis, and low (0%) rates of TD lends evidence of a psychosis spectrum conversion group [77]. The high rates of anxiety, behavior, and mood disorders persist in spite of their independence among layers indicate that these prodromal signs persist, but become decoupled [25, 72]. Uncorrelated symptoms among these subjects in NB could suggest that they tend towards psychosis through individuated channels.

PSYCHOPATHOLOGICAL SYMPTOM GROUPINGS (EARLY ADULT (18-21))

MALE								FEMALE							
	Block	<i>n</i>	Anx	Beh	Mood	TD	Psy		Block	<i>n</i>	Anx	Beh	Mood	TD	Psy
●	<i>NB</i>	41	73	95	46	0	54		<i>NB</i>	35	11	17	3	69	20
●	<i>S1</i>	244	51	39	29	30	38		<i>S1</i>	883	65	25	26	24	17
●	<i>S2</i>	471	39	21	9	42	14		<i>S2</i>	189	36	16	12	53	25

TABLE 1

Mean summary statistics for psychiatric diagnoses (approximate diagnostic criteria of DSM-IV) for early adult males and females. The following columns details symptoms of anxiety, behavior, and mood disorders. The ‘Psy’ column gives the average of whether the respondents have overall diagnoses for psychosis and the ‘TD’ column indicates typical development.

Psychosis rates are clearly differentiated between different blocks; those in NB are consistently higher. The differential clustering results for early adult males likely demonstrate latent neurodevelopmental pathways for onset of psychosis. Psychosis onset is characterized by presence of active psychotic symptoms and occurs during early adulthood between 21-25 for males [71]. This represents a continuum with individuals reporting proportionally more depression, anxiety, and behavior psychopathology prior to the onset of psychosis [25]. As symptoms segregate with growth and become statistically independent, clustered subjects with higher correlations ρ_q correspond to more interconnected pre-psychotic pathways [21], while subjects with independent symptoms are indicative of progressing past the first episode of psychosis [72, 77]. That these categories emerged without any supervision demonstrates the discerning ability of SBANM. Results did not show any strong differentiation in other demographic characteristics (Table 4 in Appendix G.3).

5.3. Method Comparison for PNC Data

We compare different community detection methods to cluster the PNC data. In the absence of ground-truth data for clusters among real data, we consider the diagnoses data of PNC subjects to validate results. The zero-correlation constraint between the layers $\mathbf{X}, \mathbf{Y}, \mathbf{Z}$ within NB discovered by SBANM is natural for testing our clinical hypothesis (Section 5). We interpret NB as the group of subjects that have transitioned from the prodromal stage to psychosis spectrum. We compare the clusters with the highest psychosis rates that was obtained from each method; we define q^* as the cluster that yields the partition of subjects with the highest rates of psychosis. Table 2 (right) compares the characteristics of q^* for each method by taking their average rates of anxiety, behavior, and mood disorders, in addition to those of psychosis and typical development (TD). Q for each method is assessed based on their own internal criteria for best fit. `dynsbm` (row 2) for example finds 8 groups based on its own ICL criteria. Optimal Q was between 3 or 4 for most spectral methods. The results of SBANM (Section 5), yielded 41 subjects in NB (q^*) with average psychosis rates of 54%. The proportion of subjects that approximate criteria for a clinical anxiety disorder from post-hoc evaluations is 73%, behavioral disorders was 95%, and 46% for mood disorders. Out of all the methods, SBANM and `dynsbm` found the clusters with the highest rates of psychosis. `dynsbm` finds a very small group (of 14 subjects) that has high rates of psychosis, anxiety, behavior, and mood disorders.

The identified clusters from `dynsbm` and *MASE*, both yield strongly positively correlated blocks across layers. Interpretating these results as symptoms transitioning from the *prodrome* to *psychosis spectrum* is less suitable. The high correlations signify high rates of co-occurrence and may correspond to the correlated prodromal symptoms that precede psychosis [77]. However, they do not capture the qualitative change that we posit as the transition from psychosis prodrome to psychosis spectrum as outlined in Section 5 [21, 25, 72]. Other methods yield results with similar rates of psychosis ($\approx 50\%$), TD ($\approx 0\%$) anxiety ($\approx 75\%$) and mood disorders ($\approx 50\%$). The spectral methods (rows 2,4,5,6) typically beget much larger groups of around one quarter to one third of the total sample size. These larger, evenly populated subgroups may yield some advantages, but reveal less specificity in terms of potential diagnosis. The constraint of independence (through zero correlation) allows a much more specific demarcation of varying psychopathologies.

We also compare multivariate spectral clustering (MVSPEC) to the PNC data that was not transformed to networks (row 6). This method did not separate subjects with psychosis nearly as well as the network methods. The degradation in classification suggests that the network transformation for large-scale questionnaire (or survey) data is perhaps even necessary for clustering analysis with the goals of diagnosis and prevention. This method was not evaluated for the simulated data.

6. Synthetic Experiments

In this section we describe the simulation studies to demonstrate the accuracy and efficacy of the proposed method. Simulations are generated to match the outcomes of the real data in the previous section. We considered networks of three layers with size 800 that match approximately with the results of early adult males. We simulate 50 networks with underlying memberships and parameters that approximately match those in Section 5. We then run SBANM on these networks to demonstrate that the method is able to recover simulated memberships and parameters. We also assess the computation times of various simulations and compare them to existing methods. The estimation algorithm is more parsimonious and highlights more nuanced relationships compared to some existing methods described in the following Section 5.

METHOD COMPARISON										
Simulations (50 Runs)			PNC Data (Male EA)							
Method	NMI	ARI	Characteristics (%) of q^* (q with highest %Psy)							
	Mean \pm SD	Mean \pm SD	Psy	TD	Anx	Beh	Mood	n_{q^*}	ρ_{q^*}	Q
SBANM	1	1	54	0	73	95	46	41	0,0,0	3
SPEC(sum)	.54 \pm .02	.53 \pm .01	51	2	77	77	49	171	-.1,-.2,.4	3
dynsbm	.98 \pm .04	.95 \pm .02	57	0	71	93	57	14	.3,.6,.7	8
MASE	.90 \pm .05	.76 \pm .09	52	5	76	55	50	139	.5,.5,.3	4
MVSPEC(net)	.66 \pm .02	.55 \pm .14	42	4	74	72	52	264	0,.1,.3	4
MVSPEC(raw)	NA	NA	33	20	62	56	42	194	NA	4

TABLE 2

Comparison of different methods for membership recovery using the ARI and NMI measures. *dynsbm* (unique config.) refers to the interpretation of the method when every unique configuration of blocks across layers are treated as a unique block. *dynsbm* (most freq.) treats the block with the most frequent occurrence of memberships across all layers as the cross-layer block. In the right column, the q^* represents cluster with highest %Psy.

6.1. Experimental Procedure

The goal of these experiments is to demonstrate that our proposed method can faithfully recover generated memberships and parameters. For this section, we write $\mu := (\mu_X, \mu_Y, \mu_Z)$ represent the means of the edge-connections for each block representing anxiety, behavior, and mood with corresponding standard deviations $\sigma = (\sigma_X, \sigma_Y, \sigma_Z)$. We let ρ represent the block-wise correlations (across all layers) $\rho := (\rho_1, \dots, \rho_Q)$. Blockwise parameters μ, σ , and ρ are extracted from the early adult males results from Section 5 to serve as the ground-truth parameters for the following experiment. Probabilities of membership-allocations τ are also extracted from the data results and used to generate multinomial distributions that approximate the “true” distributions of memberships. As such, simulated block-sizes are randomized but approximately match those of the data.

For every network, nodes are simulated within clusters with membership probabilities τ . Within these clusters, edge-weights are simulated according to the multivariate normal parameters μ, σ , and ρ . Simulated data is generated after extracting these ground-truth parameters from the results of the PNC early adult males. We set n to be 800, and then simulate a multinomial distribution of fixed total size n where each cluster has membership probabilities of 4%(NB), 32%(S_1), and 62%(S_2) from Table 1. For each mean-covariance pair corresponding to block q , we generate multivariate Gaussian distributions with a sample size of $n_q(n_q - 1)/2$, then we convert these multivariate data to weighted edges. Finally, a sample of the AN distribution with size

$$n_{IN} := (n - 1)n/2 - \sum_{q=1}^Q n_q(n_q - 1)/2$$

is generated for all n_{IN} interstitial edges between differing blocks. SBANM is then applied to these networks and we assessed membership as well as parameter recovery.

Fifty three-layer networks were generated from a fixed set of parameters and membership probabilities. For the SBANM algorithm, the initial membership probabilities τ are obtained by applying spectral clustering on the sum graph $\tilde{X}_{ij} = X_{ij} + Y_{ij} + Z_{ij}$. across all K layers, then averaged with uniformly generated probabilities. Results show consistently accurate estimates for the mean, variance, and correlation parameters (Figure 5). The algorithm was able to exactly recover memberships for all simulations ([1]). Table 2 shows that SBANM is able to retrieve the simulated memberships at a 100% recovery rate. True parameters are shown in Figure 5. The variances for most of the estimates were within 0-3% of the true values. More simulations are described in Appendix F.2.

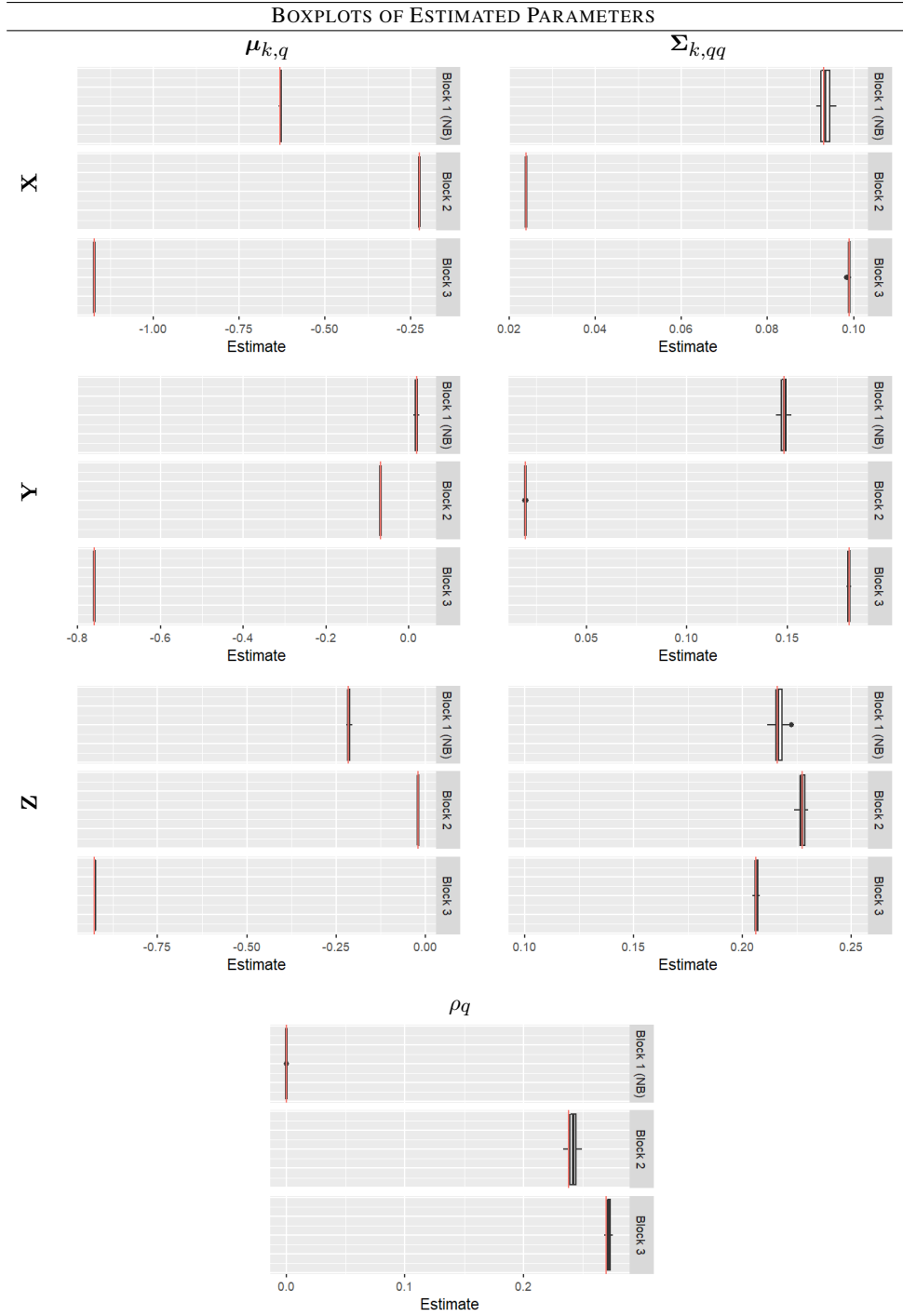


Fig 3: Boxplots for repeated estimates of simulations. We ran the algorithm applied to 100 randomly generated networks with the same ground truth parameters and sample sizes but with variable group sizes. Each boxplot represents the summary of 50 individual estimates corresponding to 50 runs. The red bands represent the ground truth parameters for means, variances, and correlations.

The only ‘free’ parameter in our algorithm is the *number of blocks* specified Q . *Model selection* in the SBM clustering context usually refers to specified Q during VEM estimation. Existing approaches [26, 50, 52] consider the *integrated complete likelihood* (ICL) for assessing block model clustering performance in weighted as well as simple graphs. We apply the method for a range of \hat{Q} (as the *estimate* for number of blocks). Results show that the usage of ICLs reaches its highest value at the correct ground truth value of 3 and verify that this metric is suitable for evaluation of the method (Figure 6 in Appendix F.3).

6.2. Method Comparisons for Synthetic Experiments

We evaluated *ARI* (Adjusted Rand Index) and *NMI* (Normalized Mutual Information) scores [52, 63, 84] for the six methods for these simulations. The scores are both between 0 and 1 and serves as a proxy for *percentage recovery*. We have found that SBANM outperforms competing methods in every setting. We note that there is perhaps some implicit bias in favor of SBANM because the simulations are generated according to the model. However, differences in recovery rates still elucidate some important information regarding the method’s efficacy.

We present these results also as a part of Table 2, earlier use for method comparison for PNC data. Table 2 (left) shows the recovery rates of the NMIs and ARIs for all of the runs of SBANM are 1, suggesting perfect recovery. Recovery rates of the spectral clustering for both the naive (single-graph sum) and multigraph spectral clustering results are around half, while *MASE* and *dynsbm* yield much better results, of up to 98% agreement. Results for other methods suggest effective *partial* recovery of the memberships from *dynsbm* and *MASE* even if none the network block structures are not perfectly recovered. None of the competing methods perfectly recover the block structures for the multilayer networks.

Computation times are also assessed for the various methods. The spectral methods (rows 2, 4, 5) of Table 2 (left) have a nearly instant run time. SBANM and *dynsbm* take longer to compute. Under the (correct) specification for $Q = 3$ SBANM, the computing time averages around 1100 seconds (in CPU time), while 350 for $Q = 2$ and 3000 for 4 blocks. For *dynsbm* the total procedure took about 3500 seconds in CPU time (with an optimal 8 clusters), which is slightly less than running SBANM for 2, 3, and 4 clusters. As such, our proposed method is fairly slow, but comparable to existing methods.

7. Discussion

We have introduced a novel method SBANM that is motivated by real-world clinical phenomenon of psychosis progression. SBANM is an unsupervised data-driven approach to identify groups of psychopathologies that describe patterns of prodromal subjects transitioning to psychosis spectrum. Future developments of method could potentially lead to a deeper understanding of the transition from prodrome to psychosis spectrum and finally to schizophrenia using statistical network theory. We demonstrated the relative benefits of this model compared to existing methods.

Network data come in complex forms. They are particularly synchronous with the surge in data availability. Our primary contribution was to introduce the notion of structured noise to weighted multilayer SBMs as well as an algorithm to estimate it. Other work has explored cases where between-block transitions are all uniquely parameterized [52], but they do not account for correlations between layers nor do they separate signal from noise. The proposed model is parsimonious and reveals more interpretable results that could be useful in clinical settings (more details in Appendix E.2). In practice, *NB* does not necessarily represent a

control group in PNC early adult males but rather a dynamic cluster that specifically captures and reflects the most notable interactions.

We have demonstrated that the method is able to uncover latent, non-trivial patterns in a psychiatric condition (as well other data in Appendices H,I). In Section 5, we have shown that SBANM reveal a moderately sized group in the male early adult age subset with high rates of psychosis spectrum incidence and, perhaps more importantly, independence across different prodromal psychopathologies. These findings are useful for the study of psychosis in its ability to separate subjects with independent prodromal conditions from those with co-occurring ones. The results from the applications to psychopathology data concurs with the ongoing discourse in moving away from *nosology* where psychiatric disorders are treated as discrete entities as opposed to multifaceted pathologies [81]. Etiologically, the proposed methodology supports the shift away from one-dimensional causal assumptions and instead to multifaceted casual pathways underlying severe psychiatric disorders such as psychosis and schizophrenia.

There are some limitations to SBANM. The issue of computation time persistently plagues variational methods. The algorithm slows when K or Q is large. However, its unique ability to partitioning independent from correlated clusters may be of more importance than speedy computation form a less nuanced method. SVI speeds up computation time to make possible what was previously infeasible. Future work may further explore subsampling methods with faster computation times.

Ambient noise in networks are related to overlapping SBMs. Some community detection methods adhere to a *bottom-up* heuristic where clusters increase in size until memberships become stable; and naturally allows for separation between *signal* and *noise*. Many of these approaches implicitly assume inherent structure but do not assign an explicitly parametric model to signal or noise [14, 63, 84]. Members not assigned to communities are called *back-ground* nodes are identified but not statistically modeled. As in many subdomains of statistics and signal processing, noise plays a large role in network theory and methods. Existing work that discusses noise in networks [57, 68, 88], mostly describe it theoretically, however, few authors specifically address noise in the context of SBMs and fewer seek to explicitly model it for practical purposes. Though our approach theoretically isolates ambient noise in that it is uncorrelated, in this study the *noise block* actually yields the most meaning.

The development of SBANM opens up many methodological avenues. One immediate next step is to expand the study of PNC data to include neuroimaging and genomics data. Such work is currently in progress for the PNC study to identify and jointly model neural and genetic influences in addition to symptoms. Another direction is in assessing significance or predictive power of the clusters. More generally, these in-group and out-of-group interactions are related to mixed effects models for multimodal weighted networks that may serve as another perspective in the study of longitudinal analysis of networks [75].

Reproducibility

Code and sample data for SBANM is available at <https://github.com/markhe1111/SBANM>.

Acknowledgements and Funding Information

This project was funded by the Rockefeller University Heilbrunn Family Center for Research Nursing (RX, 2019) through the generosity of the Heilbrunn Family. The funding organizations had no role in the design and conduct of the study; collection, management, analysis,

and interpretation of the data; preparation, review, or approval of the manuscript; and decision to submit the manuscript for publication. MH was supported by the NSDEG fellowship.

Philadelphia Neurodevelopment Cohort (PNC) clinical phenotype data used for the analyses described in this manuscript were obtained from dbGaP at <http://www.ncbi.nlm.nih.gov/sites/entrez?db=gap> through dbGaP accession [phs000607.v3.p2](#). Support for the collection of the data for Philadelphia Neurodevelopment Cohort (PNC) was provided by grant RC2MH089983 awarded to Raquel Gur and RC2MH089924 awarded to Hakon Hakonarson.

The authors thank Andrew Nobel and Shankar Bhamidi for helpful comments and theoretical advice. In particular, we thank them for defining and recognizing the problem of differential, correlated communities amongst multilayer networks. We also thank Professor Galen Reeves for helpful advice in contextualizing this work to the literature.

REFERENCES

- [1] ABBE, E. (2017). Community detection and stochastic block models: recent developments.
- [2] AIROLDI, E. M., BLEI, D. M., FIENBERG, S. E. and XING, E. P. (2007). Mixed membership stochastic blockmodels.
- [3] ALLMAN, E. S., MATIAS, C. and RHODES, J. A. (2009). Identifiability of parameters in latent structure models with many observed variables. *The Annals of Statistics* **37** 3099–3132.
- [4] ALLMAN, E. S., MATIAS, C. and RHODES, J. A. (2011). Parameter identifiability in a class of random graph mixture models. *Journal of Statistical Planning and Inference* **141** 1719–1736.
- [5] AMBROISE, C. and MATIAS, C. (2010). New consistent and asymptotically normal estimators for random graph mixture models.
- [6] ARROYO, J., ATHREYA, A., CAPE, J., CHEN, G., PRIEBE, C. E. and VOGELSTEIN, J. T. (2020). Inference for multiple heterogeneous networks with a common invariant subspace.
- [7] ARROYO RELIÓN, J. D., KESSLER, D., LEVINA, E. and TAYLOR, S. F. (2019). Network classification with applications to brain connectomics. *The Annals of Applied Statistics* **13**.
- [8] ASSOCIATION, A. P. (2013). *Diagnostic and statistical manual of mental disorders: DSM-5*, 5th ed. ed. Autor, Washington, DC.
- [9] BARBILLON, P., DONNET, S., LAZEGA, E. and BAR-HEN, A. (2015). Stochastic Block Models for Multiplex networks: an application to networks of researchers. *arXiv: Methodology*.
- [10] BENDER, E. A. and CANFIELD, A. (1978). The asymptotic number of labeled graphs with given degree sequences. *Journal of Combinatorial Theory, Series A* **24** 296–307.
- [11] BICKEL, P., CHOI, D., CHANG, X. and ZHANG, H. (2013). Asymptotic normality of maximum likelihood and its variational approximation for stochastic blockmodels. *The Annals of Statistics* **41** 1922 – 1943.
- [12] BLEI, D. M., KUCUKELBIR, A. and MCAULIFFE, J. D. (2017). Variational Inference: A Review for Statisticians. *Journal of the American Statistical Association* **112** 859–877.
- [13] BLEVINS, A. S., KIM, J. Z. and BASSETT, D. S. (2021). Variability in higher order structure of noise added to weighted networks.
- [14] BODWIN, K., ZHANG, K. and NOBEL, A. (2015). A testing-based approach to the discovery of differentially correlated variable sets.
- [15] CALKINS, M. E., MOORE, T. M., MERIKANGAS, K. R., BURSTEIN, M., SATTERTHWAITE, T. D., BILKER, W. B., RUPAREL, K., CHIAVACCI, R., WOLF, D. H., MENTCH, F., QIU, H., CONNOLLY, J. J., SLEIMAN, P. A., HAKONARSON, H., GUR, R. C. and GUR, R. E. (2014). The psychosis spectrum in a young U.S. community sample: findings from the Philadelphia Neurodevelopmental Cohort. *World Psychiatry* **13** 296–305.
- [16] CALKINS, M. E., MERIKANGAS, K. R., MOORE, T. M., BURSTEIN, M., BEHR, M. A., SATTERTHWAITE, T. D., RUPAREL, K., WOLF, D. H., ROALF, D. R., MENTCH, F. D., QIU, H., CHIAVACCI, R., CONNOLLY, J. J., SLEIMAN, P. M. A., GUR, R. C., HAKONARSON, H. and GUR, R. E. (2015). The Philadelphia Neurodevelopmental Cohort: constructing a deep phenotyping collaborative. *Journal of Child Psychology and Psychiatry* **56** 1356–1369.
- [17] CALKINS, M. E., MOORE, T. M., SATTERTHWAITE, T. D., WOLF, D. H., TURETSKY, B. I., ROALF, D. R., MERIKANGAS, K. R., RUPAREL, K., KOHLER, C. G., GUR, R. C. and GUR, R. E. (2017). Persistence of psychosis spectrum symptoms in the Philadelphia Neurodevelopmental Cohort: a prospective two-year follow-up. *World psychiatry : official journal of the World Psychiatric Association (WPA)* **16** 62—76.

- [18] CANNON, T. D., YU, C., ADDINGTON, J., BEARDEN, C. E., CADENHEAD, K. S., CORNBLATT, B. A., HEINSSSEN, R., JEFFRIES, C. D., MATHALON, D. H., MCGLASHAN, T. H., PERKINS, D. O., SEIDMAN, L. J., TSUANG, M. T., WALKER, E. F., WOODS, S. W. and KATTAN, M. W. (2016). An Individualized Risk Calculator for Research in Prodromal Psychosis. *American Journal of Psychiatry* **173** 980-988. PMID: 27363508.
- [19] CARLEN, J., DE DIOS PONT, J., MENTUS, C., CHANG, S.-S., WANG, S. and PORTER, M. A. (2019). Role Detection in Bicycle-Sharing Networks Using Multilayer Stochastic Block Models.
- [20] CAZABET, R., BORGNAT, P. and JENSEN, P. (2017). Using Degree Constrained Gravity Null-Models to understand the structure of journeys' networks in Bicycle Sharing Systems. In *ESANN 2017 - European Symposium on Artificial Neural Networks, Computational Intelligence and Machine Learning*.
- [21] CHEN, Y., FAROOQ, S., EDWARDS, J. J., CHEW-GRAHAM, C. A., SHIERS, D., FRISHER, M., HAYWARD, R. A., SUMATHIPALA, A. and JORDAN, K. P. (2019). Patterns of symptoms before a diagnosis of first episode psychosis: a latent class analysis of UK primary care electronic health records. *BMC Medicine* **17**.
- [22] CHO, Y.-S., STEEG, G. V. and GALSTYAN, A. (2011). Co-evolution of Selection and Influence in Social Networks.
- [23] CLARK, L., WATSON, D. and REYNOLDS, S. (1995). Diagnosis and classification of psychopathology: challenges to the current system and future directions. *Annual review of psychology* **46** 121—153.
- [24] CLAUSET, A., E J NEWMAN, M. and MOORE, C. (2005). Finding community structure in very large networks. *Physical review. E, Statistical, nonlinear, and soft matter physics* **70** 066111.
- [25] CUPO, L., MCILWAINE, S. V., DANEALT, J.-G., MALLA, A. K., IYER, S. N., JOOBER, R. and SHAH, J. L. (2021). Timing, Distribution, and Relationship Between Nonpsychotic and Subthreshold Psychotic Symptoms Prior to Emergence of a First Episode of Psychosis. *Schizophrenia Bulletin*. sbaa183.
- [26] DAUDIN, J. J., PICARD, F. and ROBIN, S. (2008). A mixture model for random graphs. *Statistics and Computing* **18** 173–183.
- [27] DEWASKAR, M., PALOWITCH, J., HE, M., LOVE, M. I. and NOBEL, A. (2020). Finding Stable Groups of Cross-Correlated Features in Multi-View data.
- [28] DIVVY (2019). Divvy Data.
- [29] FORTUNATO, S. and HRIC, D. (2016). Community detection in networks: A user guide. *Physics Reports* **659** 1–44.
- [30] GIRVAN, M. and NEWMAN, M. E. J. (2002). Community structure in social and biological networks. *Proceedings of the National Academy of Sciences* **99** 7821–7826.
- [31] HANDCOCK, M. S., RAFTERY, A. E. and TANTRUM, J. M. (2007). Model-based clustering for social networks. *Journal of the Royal Statistical Society: Series A (Statistics in Society)* **170** 301-354.
- [32] HE, M., GLASSER, J., BHAMIDI, S. and KAZA, N. (2020a). Intertemporal Community Detection in Human Mobility Networks.
- [33] HE, M., GLASSER, J., PRITCHARD, N., BHAMIDI, S. and KAZA, N. (2020b). Demarcating geographic regions using community detection in commuting networks with significant self-loops. *PLOS ONE* **15** e0230941.
- [34] HOFF, P. D., RAFTERY, A. E. and HANDCOCK, M. S. (2002). Latent Space Approaches to Social Network Analysis. *Journal of the American Statistical Association* **97** 1090-1098.
- [35] HOFFMAN, M., BLEI, D. M., WANG, C. and PAISLEY, J. (2012). Stochastic Variational Inference.
- [36] HOLLAND, P. W., LASKEY, K. B. and LEINHARDT, S. (1983). Stochastic blockmodels: First steps. *Social Networks* **5** 109 - 137.
- [37] HOLME, P. (2015). Modern temporal network theory: a colloquium. *The European Physical Journal B* **88**.
- [38] JAakkola, T. S. (2000). Tutorial on Variational Approximation Methods. In *IN ADVANCED MEAN FIELD METHODS: THEORY AND PRACTICE* 129–159. MIT Press.
- [39] KAHN, R., SOMMER, I., MURRAY, R., MEYER-LINDENBERG, A., WEINBERGER, D., CANNON, T., O'DONOVAN, M., CORRELL, C., KANE, J., VAN OS, J. and INSEL, T. (2015). Schizophrenia. *Nature Reviews Disease Primers* **1**.
- [40] KARRER, B. and NEWMAN, M. E. J. (2011). Stochastic blockmodels and community structure in networks. *Phys. Rev. E* **83** 016107.
- [41] KENDELL, R. and JABLENSKY, A. (2003). Distinguishing Between the Validity and Utility of Psychiatric Diagnoses. *American Journal of Psychiatry* **160** 4-12. PMID: 12505793.
- [42] KIRKBRIDE, J. B., ERRAZURIZ, A., CROUDACE, T. J., MORGAN, C., JACKSON, D., BOYDELL, J., MURRAY, R. M. and JONES, P. B. (2012). Incidence of Schizophrenia and Other Psychoses in England, 1950–2009: A Systematic Review and Meta-Analyses. *PLOS ONE* **7** 1-1.

- [43] KRABBENDAM, L., MYIN-GERMEYS, I., HANSSEN, M., DE GRAAF, R., VOLLEBERGH, W. A. M., BAK, M. and VAN OS, J. (2005). Development of depressed mood predicts onset of psychotic disorder in individuals who report hallucinatory experiences. *The British journal of clinical psychology* **44 Pt 1** 113-25.
- [44] LANCICHINETTI, A., RADICCHI, F., RAMASCO, J. J. and FORTUNATO, S. (2011). Finding Statistically Significant Communities in Networks. *PLOS ONE* **6** 1-18.
- [45] LEI, J. and LIN, K. Z. (2022). Bias-adjusted spectral clustering in multi-layer stochastic block models. *Journal of the American Statistical Association*.
- [46] LEVIN, K., ATHREYA, A., TANG, M., LYZINSKI, V., PARK, Y. and PRIEBE, C. E. (2019). A central limit theorem for an omnibus embedding of multiple random graphs and implications for multiscale network inference.
- [47] LEWIS, J. B., POOLE, K., ROSENTHAL, H., BOCHE, A., RUDKIN, A. and SONNET, L. (2020). Voteview: Congressional Roll-Call Votes Database.
- [48] LIU, S., WANG, S. and KRISHNAN, R. (2014). Persistent Community Detection in Dynamic Social Networks. In *Advances in Knowledge Discovery and Data Mining* (V. S. TSENG, T. B. HO, Z.-H. ZHOU, A. L. P. CHEN and H.-Y. KAO, eds.) 78–89. Springer International Publishing, Cham.
- [49] MACDONALD, P., LEVINA, E. and ZHU, J. (2020). Latent space models for multiplex networks with shared structure.
- [50] MARIADASSOU, M., ROBIN, S. and VACHER, C. (2010). Uncovering latent structure in valued graphs: A variational approach. *Ann. Appl. Stat.* **4** 715–742.
- [51] MATHEWS, H., MAYYA, V., VOLFOVSKY, A. and REEVES, G. (2019). Gaussian Mixture Models for Stochastic Block Models with Non-Vanishing Noise.
- [52] MATIAS, C. and MIELE, V. (2017). Statistical clustering of temporal networks through a dynamic stochastic block model. *Journal of the Royal Statistical Society: Series B (Statistical Methodology)* **79** 1119–1141.
- [53] MAYYA, V. and REEVES, G. (2019). Mutual Information in Community Detection with Covariate Information and Correlated Networks.
- [54] MC, A. and KÜHN, L. (1988). Gender differences in age at onset of schizophrenia. An overview.
- [55] MENICHETTI, G., REMONDINI, D., PANZARASA, P., MONDRAGÓN, R. J. and BIANCONI, G. (2014). Weighted Multiplex Networks. *PLOS ONE* **9** 1-8.
- [56] MERCADO, P., TUDISCO, F. and HEIN, M. (2019). Spectral Clustering of Signed Graphs via Matrix Power Means.
- [57] MIAO, R. and LI, T. (2021). Informative core identification in complex networks. *ArXiv* **abs/2101.06388**.
- [58] NEWMAN, M. E. (2003). The structure and function of complex networks. *SIAM review* **45** 167–256.
- [59] NEWMAN, M. (2018a). *Networks*. Oxford university press.
- [60] NEWMAN, M. E. J. (2018b). Estimating network structure from unreliable measurements. *Physical Review E* **98**.
- [61] NOWICKI, K. and SNIJDERS, T. A. B. (2001). Estimation and Prediction for Stochastic Blockstructures. *Journal of the American Statistical Association* **96** 1077–1087.
- [62] NOWROUZI, B., KAMHI, R., HU, J., KENNEDY, J. L., MATMARI, M. and LUCA, V. D. (2015). Age at onset mixture analysis and systematic comparison in schizophrenia spectrum disorders: Is the onset heterogeneity dependent on heterogeneous diagnosis? *Schizophrenia Research* **164** 83-91.
- [63] PALOWITZ, J., BHAMIDI, S. and NOBEL, A. B. (2018). The Continuous Configuration Model: A Null for Community Detection on Weighted Networks. *Journal of Machine Learning Research* **18** 1–48.
- [64] PAUL, S. and CHEN, Y. (2015). Community Detection in Multi-Relational Data Through Restricted Multi-Layer Stochastic Blockmodel. *preprint*.
- [65] PAUL, S. and CHEN, Y. (2018). A random effects stochastic block model for joint community detection in multiple networks with applications to neuroimaging. *preprint*.
- [66] PEIXOTO, T. P. (2018). Nonparametric weighted stochastic block models. *Phys. Rev. E* **97** 012306.
- [67] PEIXOTO, T. P. and ROSVALL, M. (2017). Modelling sequences and temporal networks with dynamic community structures. *Nature Communications* **8**.
- [68] PRIEBE, C. E., PARK, Y., VOGELSTEIN, J. T., CONROY, J. M., LYZINSKI, V., TANG, M., ATHREYA, A., CAPE, J. and BRIDGEFORD, E. (2019). On a two-truths phenomenon in spectral graph clustering. *Proceedings of the National Academy of Sciences* **116** 5995-6000.
- [69] RANGANATH, R., TRAN, D. and BLEI, D. (2016). Hierarchical Variational Models. *Proceedings of the 33rd International Conference on Machine Learning*, **18**.
- [70] REEVES, G., MAYYA, V. and VOLFOVSKY, A. (2019). The Geometry of Community Detection via the MMSE Matrix.
- [71] RENA LI, G. W. J. Y. C. W. XIN MA (2016). Why sex differences in schizophrenia? *Journal of Translational Neuroscience* **1** 37.

- [72] RENWICK, L., LYNE, J., DONOGHUE, B. O., OWENS, L., DOYLE, R., HILL, M., MCCARTHY, E., PILLING, M. A., O'CALLAGHAN, E. and CLARKE, M. C. (2015). Prodromal symptoms and remission following first episode psychosis. *Schizophrenia Research* **168** 30-36.
- [73] SALTER-TOWNSHEND, M. and MURPHY, T. B. (2013). Variational Bayesian inference for the Latent Position Cluster Model for network data. *Computational Statistics and Data Analysis* **57** 661-671.
- [74] SARKAR, P., WANG, Y. X. R. and MUKHERJEE, S. S. (2021). When random initializations help: a study of variational inference for community detection. *Journal of Machine Learning Research* **22** 1-46.
- [75] SNIJDERS, T. A. B. (2005). Models for Longitudinal Network Data. In *Models and Methods in Social Network Analysis* 215-247. University Press.
- [76] STANLEY, N., SHAI, S., TAYLOR, D. and MUCHA, P. J. (2015). Clustering Network Layers With the Strata Multilayer Stochastic Block Model. *CoRR* **abs/1507.01826**.
- [77] TANDON, N., SHAH, J. L., KESHAVAN, M. S. and TANDON, R. (2012). Attenuated psychosis and the schizophrenia prodrome: current status of risk identification and psychosis prevention. *Neuropsychiatry* **24** 345-353.
- [78] TAYLOR, D., SHAI, S., STANLEY, N. and MUCHA, P. J. (2016). Enhanced Detectability of Community Structure in Multilayer Networks through Layer Aggregation. *Phys. Rev. Lett.* **116** 228301.
- [79] TROPP, J. A. (2006). Just relax: convex programming methods for identifying sparse signals in noise. *IEEE Transactions on Information Theory* **52** 1030-1051.
- [80] VALLÈS-CATALÀ, T., MASSUCCI, F. A., GUIMERÀ, R. and SALES-PARDO, M. (2016). Multilayer Stochastic Block Models Reveal the Multilayer Structure of Complex Networks. *Phys. Rev. X* **6** 011036.
- [81] VAN PRAAG, H. M. (2000). Nosologomania: a disorder of psychiatry. *The World Journal of Biological Psychiatry* **1** 151-158.
- [82] WANG, S., ARROYO, J., VOGELSTEIN, J. T. and PRIEBE, C. E. (2019). Joint Embedding of Graphs.
- [83] WILSON, J. D., STEVENS, N. T. and WOODALL, W. H. (2019). Modeling and detecting change in temporal networks via the degree corrected stochastic block model. *Quality and Reliability Engineering International* **35** 1363-1378.
- [84] WILSON, J. D., WANG, S., MUCHA, P. J., BHAMIDI, S. and NOBEL, A. B. (2014). A testing based extraction algorithm for identifying significant communities in networks. *Annals of Applied Statistics* **8** 1853-1891.
- [85] YAN, X., SHALIZI, C., JENSEN, J. E., KRZAKALA, F., MOORE, C., ZDEBOROVA, L., ZHANG, P. and ZHU, Y. (2014). Model selection for degree-corrected block models. *Journal of Statistical Mechanics: Theory and Experiment* **5** 05-07.
- [86] YIN, M., WANG, Y. X. R. and SARKAR, P. (2020). A Theoretical Case Study of Structured Variational Inference for Community Detection. In *AISTATS*.
- [87] YOUNG, J.-G., CANTWELL, G. T. and NEWMAN, M. E. J. (2020). Bayesian inference of network structure from unreliable data. *Journal of Complex Networks* **8**.
- [88] ZHANG, Z., ZHENG, Z., NIU, H., MI, Y., WU, S. and HU, G. (2015). Solving the inverse problem of noise-driven dynamic networks. *Phys. Rev. E* **91** 012814.
- [89] ZHAO, Y., LEVINA, E. and ZHU, J. (2012). Consistency of community detection in networks under degree-corrected stochastic block models. *Ann. Statist.* **40** 2266-2292.
- [90] ZHOU, F., XU, X., ZHANG, K., TRAJCEVSKI, G. and ZHONG, T. (2020). Variational Information Diffusion for Probabilistic Cascades Prediction. In *IEEE INFOCOM 2020 - IEEE Conference on Computer Communications* 1618-1627. IEEE Press.

Supplementary Material for Community Detection in Weighted Multilayer Networks with Ambient Noise

APPENDIX A: PROOFS AND DERIVATIONS

In this appendix we provide the proofs and derivations for the terms for the algorithm updates in Section 4. Note that in Appdenices **A**, **B** and **C** we use slightly different notation: instead of \mathcal{X} and \mathcal{Z} for data and membership matrices, we revert to that used by other work and instead use \mathbf{X} and \mathbf{Z} . Note that this notation interferes with the layers of the network in in the PNC case study, but for these first three appendices they are representative of more general cases.

A.1. Proof for Hierarchical ELBO

This is a proof paraphrased from Ranganath et al. [69] that the hierarchical ELBO is a sharper lower bound than the ELBO. An inequality can be drawn between the “ordinary” ELBO \mathcal{L} without any hierarchical information and the Hierarchical ELBO

$$\begin{aligned}\mathcal{L} &= \mathbb{E}_{R_{\text{hv}}(\mathbf{Z})} [\log f(\mathbf{Z}, \mathbf{X})] + \mathcal{H}_{\text{hv}}(R(\mathbf{Z})) \\ &\geq \mathbb{E}_{R(\mathbf{Z}, \mathbf{C})} [\log f(\mathbf{Z}, \mathbf{X})] - \mathbb{E}_{R(\mathbf{Z}, \mathbf{C})} [\log R(\mathbf{Z}, \mathbf{C})] + \mathbb{E}_{R(\mathbf{Z}, \mathbf{C})} [\log S(\mathbf{C}|\mathbf{Z})] \\ &:= \mathcal{L}'(\text{Hierarchical ELBO}).\end{aligned}$$

The inequality in the above relationship arises from the decomposition of the entropy \mathcal{H}_{hv} of the hierarchical distribution. The proof of the inequality is based on the proof from Ranganath et al. [69] :

PROPOSITION 1.

$$\mathcal{H}_{\text{hv}}(R(\mathbf{Z})) \geq -\mathbb{E}_{R(\mathbf{Z}, \mathbf{C})} [\log R(\mathbf{Z}, \mathbf{C})] + \mathbb{E}_{R(\mathbf{Z}, \mathbf{C})} [\log S(\mathbf{C}|\mathbf{Z})].$$

PROOF.

$$\begin{aligned}\mathcal{H}_{\text{hv}}(R(\mathbf{Z})) &= -\mathbb{E}_{R_{\text{hv}}(\mathbf{Z})} [\log R_{\text{hv}}(\mathbf{Z})] \\ &= -\mathbb{E}_{R_{\text{hv}}(\mathbf{Z})} [\log R_{\text{hv}}(\mathbf{Z}) - \mathbf{KL}(R_{\mathbf{C}|\mathbf{Z}}(\mathbf{C}|\mathbf{Z}); R_{\mathbf{C}|\mathbf{Z}}(\mathbf{C}|\mathbf{Z}))] \\ &\geq -\mathbb{E}_{R_{\text{hv}}(\mathbf{Z})} [\log R_{\text{hv}}(\mathbf{Z}) + \mathbf{KL}(R_{\mathbf{C}|\mathbf{Z}}(\mathbf{C}|\mathbf{Z}); S(\mathbf{C}|\mathbf{Z}))] \\ &= -\mathbb{E}_{R_{\text{hv}}} [\mathbb{E}_{R(\mathbf{Z})} [\log R_{\text{hv}}(\mathbf{Z})] + \log R_{\mathbf{C}|\mathbf{Z}}(\mathbf{C}|\mathbf{Z}) - \log S(\mathbf{C}|\mathbf{Z})] \\ &= -\mathbb{E}_{R(\mathbf{Z}, \mathbf{C})} [\log R_{\text{hv}}(\mathbf{Z}) + \log R_{\mathbf{C}|\mathbf{Z}}(\mathbf{C}|\mathbf{Z}) - \log S(\mathbf{C}|\mathbf{Z})] \\ &= -\mathbb{E}_{R(\mathbf{Z}, \mathbf{C})} [\log R_{\mathbf{Z}, \mathbf{C}}(\mathbf{Z}, \mathbf{C}) - \log S(\mathbf{C}|\mathbf{Z})]\end{aligned}$$

□

A.2. Preservation of $\mathbb{E}_{R(\mathbf{Z}, \mathbf{C})} [\log f(\mathbf{Z})]$

Here we show that the term for $\mathbb{E}_{R(\mathbf{Z}, \mathbf{C})} [\log f(\mathbf{Z})]$ as written in Eq. (10) is the same as in prior studies such as Daudin et al. [26]

PROPOSITION 2.

$$\mathbb{E}_{R(\mathbf{Z}, \mathbf{C})} [\log f(\mathbf{Z})] = \sum_{i,q} \tau_{iq} \log \alpha_q$$

PROOF.

$$\begin{aligned}\mathbb{E}_{R(\mathbf{Z}, \mathbf{C})} [\log f(\mathbf{Z})] &= \sum_i \sum_q \left(P_q \tau_{iq} \log \alpha_q + (1 - P_q) \tau_{iq} \log \alpha_q \right) \\ &= \sum_q (P_q + (1 - P_q)) \left(\sum_i \tau_{iq} \log \alpha_q \right) \\ &= \sum_{i,q} \tau_{iq} \log \alpha_q.\end{aligned}$$

□

A.3. Derivation for Expected Log Likelihood

Description of the form of the joint likelihood in Equation (12) in Section ??:

PROPOSITION 3. *The expected log likelihood of the multivariate normal distribution $f(\mathbf{Z}, \mathbf{C})$ with respect to $R(\mathbf{Z}, \mathbf{C})$ is written as*

$$\mathbb{E}_{R(\mathbf{Z}, \mathbf{C})}[\log f(\mathbf{X}, \mathbf{Z})] = \mathbb{E}_{R(\mathbf{Z}, \mathbf{C})}[\log f(\mathbf{X}|\mathbf{Z})] + \sum_i \sum_q \tau_{iq} \log \alpha_q$$

PROOF.

$$\begin{aligned} \mathbb{E}_{R(\mathbf{Z}, \mathbf{C})}[\log f(\mathbf{X}, \mathbf{Z})] &= \mathbb{E}_{R(\mathbf{Z}, \mathbf{C})}[\log f(\mathbf{X}|\mathbf{Z})] + \mathbb{E}_{R(\mathbf{Z}, \mathbf{C})}[\log f(\mathbf{Z})] \\ &= \mathbb{E}_{R(\mathbf{Z}, \mathbf{C})}[\log f(\mathbf{X}|\mathbf{Z})] + \log \Psi \sum_i \sum_q P_q \tau_{iq} \log \alpha_q \\ &\quad + \log(1 - \Psi) \sum_i \sum_q (1 - P_q) \tau_{iq} \log \alpha_q \\ &= \mathbb{E}_{R(\mathbf{Z}, \mathbf{C})}[\log f(\mathbf{X}|\mathbf{Z})] + \sum_{i,q} \left(P_q \tau_{iq} \log \alpha_q + (1 - P_q) \tau_{iq} \log \alpha_q \right) \\ (15) \quad &= \mathbb{E}_{R(\mathbf{Z}, \mathbf{C})}[\log f(\mathbf{X}|\mathbf{Z})] + \sum_{i,q} \tau_{iq} \log \alpha_q \end{aligned}$$

□

A.4. Derivation of Joint Distribution $\mathbb{E}_{R(\mathbf{Z}, \mathbf{C})}[\log R(\mathbf{Z}, \mathbf{C})]$

The expectation of the log of the joint variational distribution is as follows:

$$\begin{aligned} \mathbb{E}_{R(\mathbf{Z}, \mathbf{C})}[\log R(\mathbf{Z}, \mathbf{C})] &= \mathbb{E}_{R(\mathbf{Z}, \mathbf{C})}[\log R(\mathbf{Z}|\mathbf{C})] + \mathbb{E}_{R(\mathbf{Z}, \mathbf{C})}[\log R(\mathbf{C})] \\ &= \sum_{i,q} \left((1 - P_q) \mathbb{E} Z_{iq} \log(\tau_{iq}) + P_q \mathbb{E} Z_{iq} \log(\tau_{iq}) \right) + \mathbb{E}[\log R(\mathbf{C})] \\ &= \sum_{i,q} \tau_{iq} \log \tau_{iq} + \sum_q \left(P_q \log P_q + (1 - P_q) \log(1 - P_q) \right) \end{aligned}$$

APPENDIX B: ELBO AND HIERARCHICAL ELBO

This section contains details for the hierarchical ELBO as well as the derivations for these expressions. The definition of ELBO is as follows:

DEFINITION 5. (*Evidence Lower Bound (ELBO)*) *Given observed data \mathbf{X} with unknown latent membership variables \mathbf{Z} , the evidence lower bound (ELBO) \mathcal{L} is the approximately optimal likelihood that minimizes the KL Divergence between the approximate distribution $R(\mathbf{Z}, \mathbf{C})$ and the posterior frequency $f(\mathbf{Z}, \mathbf{C}|\mathbf{X})$. It is expressed as follows:*

$$\mathcal{L} = \mathbb{E}_{R_{hv}(\mathbf{Z})} [\log f(\mathbf{Z}, \mathbf{X}) - \log R_{hv}(\mathbf{Z})]$$

Alternatively, the ELBO can be rewritten as the sum of the expected frequency and the entropy \mathcal{H} of variational variable \mathbf{Z} :

$$\mathcal{L} = \mathbb{E}_{R_{hv}(\mathbf{Z})} [\log f(\mathbf{Z}, \mathbf{X})] + \mathcal{H}_{hv}(R(\mathbf{Z})).$$

In Appendix A.1 we have shown the inequality between the “ordinary” ELBO \mathcal{L} and Hierarchical ELBO \mathcal{L}' . We write \mathcal{L}' here as follows:

$$\mathcal{L}' = \mathbb{E}_{R(\mathbf{Z}, \mathbf{C})} [\log f(\mathbf{Z}, \mathbf{X})] - \mathbb{E}_{R(\mathbf{Z}, \mathbf{C})} [\log R(\mathbf{Z}, \mathbf{C})] + \mathbb{E}_{R(\mathbf{Z}, \mathbf{C})} [\log S(\mathbf{C}|\mathbf{Z})]$$

B.1. Log likelihood Part of Hierarchical ELBO

The log likelihood portion of the hierarchical ELBO is written as :

$$\begin{aligned} \mathbb{E}_{R_{\mathbf{X}}} [\log(f(\mathbf{X}|\mathbf{Z}))] &= \sum_q P_q \sum_i \sum_j \tau_{iq} \tau_{jq} \left(\frac{1}{2} (\mathbf{X}_{ij} - \boldsymbol{\mu}_q)^T \boldsymbol{\Sigma}_q^{-1} (\mathbf{X}_{ij} - \boldsymbol{\mu}_q) - (2\pi)^{K/2} (\log |\boldsymbol{\Sigma}_q|)^{1/2} \right) \\ &+ \sum_q (1 - P_q) \sum_i \sum_j \tau_{iq} \tau_{jq} \left(\frac{1}{2} (\mathbf{X}_{ij} - \boldsymbol{\mu}_{AN})^T \boldsymbol{\Sigma}_{AN}^{-1} (\mathbf{X}_{ij} - \boldsymbol{\mu}_{AN}) - (2\pi)^{K/2} (\log |\boldsymbol{\Sigma}_{AN}|)^{1/2} \right) \\ &+ \sum_q \sum_{l:l \neq q} \sum_i \sum_j \tau_{iq} \tau_{jl} \left(\frac{1}{2} (\mathbf{X}_{ij} - \boldsymbol{\mu}_{AN})^T \boldsymbol{\Sigma}_{AN}^{-1} (\mathbf{X}_{ij} - \boldsymbol{\mu}_{AN}) - (2\pi)^{K/2} (\log |\boldsymbol{\Sigma}_{AN}|)^{1/2} \right). \end{aligned}$$

B.2. Expression for Hierarchical ELBO

The full form of the hierarchical ELBO is the log likelihood part (Section B.1) plus the membership probabilities, entropy, and their hierarchical counterparts:

$$\begin{aligned} \mathcal{L}' &= \mathbb{E}_{R_{\mathbf{X}}} [\log(f(\mathbf{X}|\mathbf{Z}))] + \sum_{i,q} \tau_{iq} \log \alpha_q - \sum_q \sum_i \tau_{iq} \log \tau_{iq} - \\ &\sum_q \left(P_q \log P_q + (1 - P_q) \log(1 - P_q) \right) + \sum_i \sum_q \left(P_q \log \Psi + (1 - P_q) \log(1 - \Psi) \right) \tau_{iq} \end{aligned}$$

This is the full expression for the hierarchical ELBO as described in Section 3.2.

APPENDIX C: CALCULATIONS FOR VARIATIONAL EM ALGORITHM

This section gives derivations for every step of the Variational EM algorithm in Section 4.

C.1. Optimizing Membership Probabilities τ in E-Step

We find optimal values for each τ_{iq} by solving this following equation, which is described in Section 4.1:

$$\begin{aligned} \frac{\partial}{\partial \tau_{iq}} \mathcal{L} &= \log(\alpha_q) + \sum_{k \leq K} \sum_{j \leq n} \tau_{jl} \left(P_q f(X_{ij}^k, \boldsymbol{\mu}_q, \boldsymbol{\Sigma}_q) + (1 - P_q) f(X_{ij}^k, \boldsymbol{\mu}_{AN}, \boldsymbol{\Sigma}_{AN}) \right. \\ &\quad \left. + \sum_{l \leq Q: l \neq q} f(X_{ij}^k, \boldsymbol{\mu}_{AN}, \boldsymbol{\Sigma}_{AN}) \right) - \log(\tau_{iq}) - 1 + P_q \log \Psi + (1 - P_q) \log(1 - \Psi) \\ &:= 0, \end{aligned}$$

rearranging τ_{iq} we solve this equation using a fixed point iteration procedure

C.2. Estimation of Noise Probability P_q in E-Step

Variational variables P_q that serve as the “soft” versions of C_q can be approximated by estimating the probability of block q being a “signal” block or noise block. The terms $\mathbb{E}_{R(\mathcal{Z}, \mathbf{C})} \log f(\mathbf{X}|\mathbf{Z})$, $\mathbb{E}[\log R(\mathbf{C})]$, $\mathbb{E}[\log S(\mathbf{C}|\mathbf{Z})]$ in \mathcal{L}' are dependent on \mathbf{C} . Practically, because we need to normalize for N_q , which is $1 - P_q$, that variable is more simple (if not the only possible tractable option).

$$\begin{aligned} \frac{\partial}{\partial N_q} \mathcal{L}' &= \frac{\partial}{\partial N_q} \mathbb{E}_{R(\mathcal{Z}, \mathbf{C})} [\log f(\mathbf{X}|\mathbf{Z})] - \log N_q + \log(1 - N_q) - (\log \Psi + \log(1 - \Psi)) \sum_i \tau_{iq} \\ &:= 0 \end{aligned}$$

where the first term is $f(\cdot)$ is the portion of the multivariate normal density as described in Section B.1.

$$\sum_k \sum_{i,j} \tau_{iq} \tau_{jq} \left(f(X_{ij}^k, \boldsymbol{\mu}_q, \boldsymbol{\Sigma}_q) - f(X_{ij}^k, \boldsymbol{\mu}_{AN}, \boldsymbol{\Sigma}_{AN}) + \log \left(\frac{1 - \Psi}{\Psi} \right) \right) = \log \left(\frac{N_q}{1 - N_q} \right)$$

So then, after rearranging:

$$\widehat{N}_q = \left(1 + \left[\exp \left(\sum_k \sum_i \sum_j \tau_{iq} \tau_{jq} \left(f(X_{ij}^k, \boldsymbol{\mu}_q, \boldsymbol{\Sigma}_q) - f(X_{ij}^k, \boldsymbol{\mu}_{AN}, \boldsymbol{\Sigma}_{AN}) + \log \left(\frac{1 - \Psi}{\Psi} \right) \right) \right) \right]^{-1} \right)^{-1}.$$

Then the final N_q estimates are made after normalizing all \widehat{N}_q such that they sum to one. Finally, the P_q estimates are made by subtracting N_q from 1.

C.3. Derivation of Signal Terms for M-Step

The closed-form estimate of the parameter for the mean vector $\boldsymbol{\mu}_q$ for each block q from the M-step is

$$\begin{aligned} \widehat{\boldsymbol{\mu}}_q &= \frac{\sum_{i,j} \tau_{iq} \tau_{jq} \mathbf{X}_{ij}}{\sum_{i,j} \tau_{iq} \tau_{jq}} P_q + \frac{\sum_{i,j} \tau_{iq} \tau_{jq} \boldsymbol{\mu}_{AN}}{\sum_{i,j} \tau_{iq} \tau_{jq}} \cdot (1 - P_q) \\ &= \frac{\sum_{i,j} \tau_{iq} \tau_{jq} \mathbf{X}_{ij}}{\sum_{i,j} \tau_{iq} \tau_{jq}} P_q + \boldsymbol{\mu}_{AN} (1 - P_q) \end{aligned}$$

Assuming convergence of P_q to either 0 or 1 within the context of the variational iterations, the theoretical value of

$$\boldsymbol{\mu}_q = \begin{cases} \frac{\sum_{i,j} \tau_{iq} \tau_{jq} \mathbf{X}_{ij}}{\sum_{i,j} \tau_{iq} \tau_{jq}} & \text{if } q \text{ is Signal: } P_q = 1 \\ \boldsymbol{\mu}_{AN} & \text{if } q \text{ is Noise: } P_q = 0 \end{cases}$$

Similarly to mean calculations, the variance calculations (along diagonals) are :

$$\begin{aligned} \widehat{\boldsymbol{\Sigma}}_q &= \frac{\sum_{i,j} \tau_{iq} \tau_{jq} (\mathbf{X}_{ij} - \boldsymbol{\mu}_q)^2}{\sum_{i,j} \tau_{iq} \tau_{jq}} \cdot P_q + \boldsymbol{\Sigma}_{AN} \cdot (1 - P_q) \\ &= \begin{cases} \sum_{i,j} \tau_{iq} \tau_{jq} (\mathbf{X}_{ij} - \boldsymbol{\mu}_q)^2 / \sum_{i,j} \tau_{iq} \tau_{jq} & \text{if } q \text{ is Signal: } P_q = 1 \\ \boldsymbol{\Sigma}_{AN} & \text{if } q \text{ is Noise: } P_q = 0 \end{cases} \end{aligned}$$

The cross-term for two layers h, k is written as:

$$\begin{aligned}\widehat{\Sigma}_{hk,q} &= \frac{\sum_{i,j} \tau_{iq} \tau_{jq} (\mathbf{X}_{k,ij} - \boldsymbol{\mu}_{q,k})(\mathbf{X}_{ij}^h - \boldsymbol{\mu}_{q,h})}{\sum_{i,j} \tau_{iq} \tau_{jq}} \cdot P_q + 0 \cdot (1 - P_q) \\ &= \frac{\sum_{i,j} \tau_{iq} \tau_{jq} (\mathbf{X}_{ij}^k - \boldsymbol{\mu}_{q,k})(\mathbf{X}_{ij}^h - \boldsymbol{\mu}_{q,h})}{\sum_{i,j} \tau_{iq} \tau_{jq}} \cdot P_q\end{aligned}$$

The element-wise correlations at iteration t across layers h, k ($h \neq k$) are then calculated as

$$\hat{\rho}_q^{h,k} = \frac{\widehat{\Sigma}_{hk}^q}{\sqrt{\widehat{\Sigma}_q^h \widehat{\Sigma}_q^k}}.$$

Finally, the putative correlation (across all layers) for block q is

$$\hat{\rho}_q = \max_{h,k} \hat{\rho}_q^{h,k}.$$

C.4. Derivation for $\boldsymbol{\mu}_{AN}$ and Σ_{AN}

This is derivation for (4.2.1) To calculate the global parameters, the global noise probability term Ψ defined previously is

$$\begin{aligned}\widehat{\boldsymbol{\mu}_{AN}} &= \mathbb{E}_{R(\mathbf{Z}, \mathbf{C})} [\boldsymbol{\mu}_{AN}] \\ &= \mathbb{P}(B_q \neq NB) \mathbb{E}_{R(\mathbf{Z}, \mathbf{C})} [\boldsymbol{\mu}_{AN} | B_q \text{ is not } NB] \\ &\quad + \mathbb{P}(B_q = NB) \mathbb{E}_{R(\mathbf{Z}, \mathbf{C})} [\boldsymbol{\mu}_{AN} | \{B_q = NB\}]; \quad q : 1 \leq q \leq Q \\ &= \Psi \frac{\sum_{j,i} \sum_{l,q:q \neq l} \tau_{iq} \tau_{jl} \mathbf{X}_{ij}}{\sum_{j,i} \sum_{l,q:q \neq l} \tau_{iq} \tau_{jl}} + (1 - \Psi) \frac{\sum_{j,i} \sum_q \tau_{iq} \tau_{jq} (1 - P_q) \mathbf{X}_{ij}}{\sum_{j,i} \sum_q \tau_{iq} \tau_{jq} (1 - P_q)},\end{aligned}$$

$\widehat{\Sigma}_{AN}$ can also be calculated in a similar way.

C.5. Derivation of Ψ

In this section we derive Ψ Let $\{NB\}$ represent the event that there exists a Noise Block in the multilayer graph system. The we write the indicator for this event as $\mathbf{1}(NB)$ with probability $\mathbb{P}(NB)$.

$$\begin{aligned}\Psi &= \mathbb{P}(B_q \neq NB; \forall q : q \leq Q) \\ &= \mathbb{P}(C_q = 1; \forall q : q \leq Q) \\ &= 1 - \mathbb{P}(\text{Global average rate of } q \text{ s.t. } C_q = 0; \forall q : q \leq Q) \\ &= 1 - 1/Q \\ &= (Q - 1)/Q\end{aligned}$$

APPENDIX D: STOCHASTIC VARIATIONAL INFERENCE

. To speed up computation, we apply stochastic variational inference (SVI) to calculate the membership parameters τ_{iq} and P_q . We subsample nodes at each step of the E-step in variational EM. Calculating $\tau_{iq,t}$ and $P_{q,t}$ comprise two stochastic sub-steps of the E-step at iteration step t ; we label their SVI estimates as $\hat{\tau}_{iq,t}$ and $\hat{P}_{q,t}$. At each t , we sample a set of nodes $M = \{i_1, \dots, i_m\}$ of size m and their associated edges from graph layers $\mathbf{X}^1, \dots, \mathbf{X}^K$. Let $\tau_{iq,t}^m$ represent the randomly subsampled graph at iteration step t .

1. (Calculating $\tau_{iq,t}^m$) Partial updating step for $\tau_{iq,t}^*$ at time t wherein the subsampled memberships $i, j \in M$ are found:

$$\tau_{iq,t}^* \propto \exp \left(\log(\alpha_q) + \sum_{k \leq K} \sum_{j, l \in M} \tau_{jl,t-1} \left(P_q f(X_{ij}^k, \boldsymbol{\mu}_q, \boldsymbol{\Sigma}_q) + (1 - P_q) f(X_{ij}^k, \boldsymbol{\mu}_{AN}, \boldsymbol{\Sigma}_{AN}) \right. \right. \\ \left. \left. + \sum_{l: l \neq q} f(X_{ij}^k, \boldsymbol{\mu}_{AN}, \boldsymbol{\Sigma}_{AN}) \right) - 1 + P_q \log \Psi + (1 - P_q) \log(1 - \Psi) \right).$$

The update step averages the newly calculated $\tau_{iq,t}^*$ with the previous value

$$\hat{\tau}_{iq,t} = \delta_t \tau_{iq,t}^* + (1 - \delta_t) \hat{\tau}_{iq,t-1}.$$

2. (Calculating $P_{q,t}$) The signal probability P_q is calculated in (13) but with the same subsampled replacements as done in the previous calculation of $\boldsymbol{\tau}$. For each time point the new noise probability $p_{q,t}^*$ is calculated and averaged with the previous noise probability at time $t - 1$. The update step is

$$\hat{P}_{q,t} = \delta_t P_{q,t}^* + (1 - \delta_t) \hat{P}_{q,t-1}.$$

D.1. Details on Stochastic Variational Inference

To apply stochastic variational inference, we first define the time-variable *subsampling parameter* δ_t to retain some memory from previous iteration. At every step t , a subsampled index set $B(\delta_t) \in [n]$ is randomly drawn from the data, then the step of the algorithm is only applied to the subsample $\mathbf{X}_{B(\delta_t)}$. A time-varying $\delta_t \in (0, 1)$ is selected to satisfy the convexity assumption of (1) $\sum_t \delta_t = \infty$ and (2) $\sum_t \delta_t^2 < \infty$ as outlined in [35], for some $\kappa \in (.5, 1)$

$$\delta_t = (t + 1)^{-\kappa}.$$

However, this criteria needs to be changed when the stochastically sampled variables represent memberships. Empirically, the samples converge at a fast rate when the initial “burn in” steps are subsampled, with subsample sizes increasing with each successive step. If subsampling does not take place, a potentially major impediment may arise from the slow computation speed in early steps where initialized estimates are not near the optimal values. As such, the step sizes are set as such:

$$\delta_t = \min \left(a + \left(\frac{t}{t+1} \right)^\kappa, n, n \right).$$

a and κ are constants. a governs the smallest subsample size and $\kappa > 1$ governs the rate of increase for subsample size at each step size, with the maximum possible subsample size n . A larger a means a larger starting subsample, and a larger κ means a faster rate of increase in subsample size.

Empirically, for a wide range of simulations, an effective choice for a is between 100 to 200 (depending on network size) and for κ is 2. These values are chosen to ensure computational efficiency in addition to accuracy: computation times for initial values are much slower if the parameter estimates are far from the optimal values which maximize the ELBO, so smaller sample sizes in earlier iterations will economize computation by producing more local minima, while later iterations will yield more globally accurate estimates [35].

APPENDIX E: IDENTIFIABILITY AND PARSIMONY

E.1. Identifiability and Connection to Prior Models

In the introduction, we reference the *affiliation model* in Section 1.1 as an example of prior work describing global noise on networks. On a single weighted network, a simple parametric model known as the affiliation model described in Allman et al. [4] is formulated as follows with piecewise global fixed rates:

$$\mu_{ql} = (1 - p_{ql})\delta_0 + p_{ql}F_{ql}(\theta_{\text{in}}\mathbf{1}_{q=l} + \theta_{\text{out}}\mathbf{1}_{q \neq l}); \quad 1 \leq q, l \leq Q$$

where probability p_{ql} is the sparsity parameter, continuous distribution $F_{ql}(\theta_{ql})$ with parameter θ_{ql} and δ_0 is a dirac mass at zero, and with probability

$$p_{ql} = \alpha\mathbf{1}_{q=l} + \beta\mathbf{1}_{q \neq l}; \quad .$$

One can conceive of the weighted stochastic blockmodel as a special case of the *general form of mixture models for random graphs* described in [4]. For graph X where each weighted edge is X_{ij} between nodes i, j :

$$\forall q, l \in \{1, \dots, Q\} \quad X_{ij} | \{Z_{iq}Z_{jl} = 1\} \sim p_{ql}f(\cdot, \theta_{ql}) + (1 - p_{ql})\delta_0(\cdot),$$

where p_{ql} serves as the sparsity parameter between 0 and 1, which represents the proportion of \cdot . $f(\cdot, \theta_{ql})$ represents the parametric family of distributions at specified in group-interactions q and l . The conditional distribution of X_{ij} is a mixture of the Dirac distribution at zero representing non-present edges. The proposed SBANM model can also be viewed as an instance of the generalized model above. It is a mixture of the affiliation model and the weighted multilayer SBM. Matias et al. [52] discuss identifiability of block parameters in multilayer SBMs. The authors cite [4] in setting the conditions for identifiability for weighted SBMs over multiple layers. Since the affiliation model is also proven to be identifiable [3], we posit that SBANM is also identifiable.

In practice, the membership and parameter recovery in simulations in Section 6.1 suggests that the model is identifiable empirically. However, theoretical justifications may be pursued in future work.

E.2. Parsimony Compared to Other Models

SBANM is a parsimonious compared to most other models. If inter-block interactions ($B_q \neq B_l$) are all unique, as in some models [50, 52] then this lends to overparametrization, especially at high dimensions ($\approx K \times \frac{Q(Q-1)}{2}$ parameters). The number of parameters may be reasonable for binary and Poisson-distributed multilayer networks, but will quickly inflate in the multivariate Gaussian case. SBANM yields $2KQ + Q - 1 + 2K$ parameters comprising the $2KQ$ mean and (diagonal elements of) variance parameters $\{(\mu_q, \Sigma_q)\}_{q:q \leq Q}$, $Q - 1$ correlation parameters $\{\rho_q\}_{q:q \leq Q, q \neq q_{NB}}$, and $2K$ noise parameters (μ_{AN}, Σ_{AN}) . As Q becomes large, the number of parameters increases quadratically in the canonical weighted SBM but linearly in SBANM. As K becomes large, also, the rate of increase for parameters in the proposed method is smaller than that in existing methods. This advantage is demonstrated in computing time comparisons in Section 6.3.1.

APPENDIX F: ADDITIONAL SIMULATIONS

In this section, we describe three additional simulations that were conducted for the proposed method. The experiment applies the proposed method on simulations with varying parameters. The second experiment applies the method to networks generated from the same

parameters. The third experiment verifies the usage of the *integrated composite likelihood* [52] selecting the optimal Q^* . Finally, the last section runs the method on some larger networks.

F.1. Simulations of Networks with Differing Parameters (Experiment 1)

We first describe the simulation scheme of the first experiment. The means for each unique block for every network are randomly generated from a Gaussian distribution centered around 0 and 2 respectively for the first and second layers. After the parameters are generated, the observations are simulated from multinormal distributions governed by these parameters. Each network has AN governing both a single block NB and interstitial noise IN that is centered around $(-1,0)$. We repeat this procedure for trivariate networks of $n = 200$ nodes, wherein the Gaussian priors for each (signal) block have means of -2, 0, and 2 respectively for the first, second, and third layers. In order to ensure the separability of blocks during simulations, we only select the networks whose blocks' minimum Bhattacharya distances are above a certain threshold. We calculate the minimum Bhattacharya distances between blocks across 500 simulated networks, and then select the networks with the largest 10% of the minimum Bhattacharya distances to filter out the networks whose blocks are 'far enough away' from each other; we run 50 instances of the SBANM algorithm for both the bivariate ($n = 500$) and the trivariate case ($n = 200$).

Results

Fifty runs of the algorithm were performed for both the bivariate and trivariate networks with differing parameters. 500 networks were generated as described in the previous section, then networks with the highest 10% of the minimum Bhattacharya Distances between clusters' parameters are retained.

Though this experiment is primarily focused on *membership recovery*, parameter estimation remains as a byproduct. Across many simulations with a variety of parameters, there does not seem to be much systemic bias in the estimates as empirical means of differences between estimated and true parameters are centered around 0. Median percentage differences, across all estimated parameters, between the estimates and true values are between 20 to 25% for bivariate, and 10-20% for trivariate networks. Histograms for the mean and variance parameters (each distinct parameter is treated like an observation) show essentially matching distributions between estimates and ground truth parameters for means (4).

A slight discrepancy between distributions for variance parameters ($\sigma_{q,k}^2$ for $k = 1, 2, 3$) among trivariate networks. This slight bias may be related again to the curse of dimensionality and, while does not seem to elicit too severe a problem in the clustering results, may be investigated in future endeavors.

Percentage differences between the estimated and ground-truth parameters also show moderately accurate recovery in both bivariate and trivariate networks. The lowest 25% quartiles for all parameters are between 0 and 3 percent and show that these estimates are very close to the ground truths. Conflated with the relatively higher mean and median differences, the low 1st quartiles show that accuracy for parameter runs seem to occur along a binary: either estimates are very close to their targets, or they are fairly far off. Some of the high percentage differences may arise from small ground-truth values, which are divided to calculate percentage differences. Others may arise from the mismatches in clustering memberships. However, this limitation mostly arises in the trivariate case, as there is a near-perfect recovery rate for the bivariate simulations.

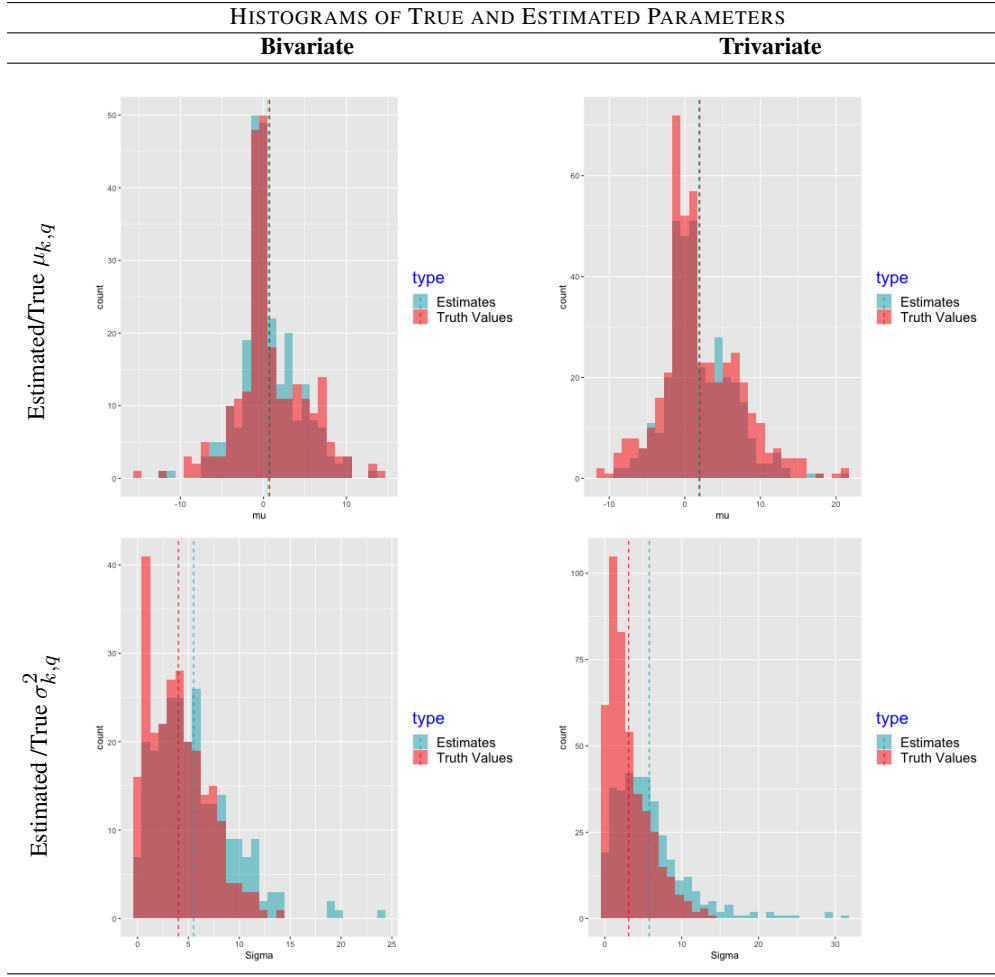


Fig 4: Histograms of ground truth (red) and estimate (blue) parameter values for the 2-layer and 3-layer networks compared to the estimated parameters from the algorithm. Parameters across layers are all plotted together. Dashed lines demarcate the empirical means of these estimated and ground truth parameters. For ground truths (red), these empirical means are .75 for $\mu_{k,q}$ (bivariate, top left), 1.98 for $\mu_{k,q}$ (trivariate, top right), 4.01 for $\sigma_{k,q}^2$ (bivariate, bottom left), 3.10 for $\sigma_{k,q}^2$ (trivariate, bottom right). For estimates of parameters, they are .58 for $\mu_{k,q}$ (bivariate, top left), 1.84 for $\mu_{k,q}$ (trivariate, top right), 5.51 for $\sigma_{k,q}^2$ (bivariate, bottom left), 5.58 for $\sigma_{k,q}^2$ (trivariate, bottom right).

F.2. Simulations of Networks with the Same Parameters (Experiment 2)

The first experiment was conducted primarily to demonstrated membership recovery under a variety of different parameters and block sizes. The purpose of the second experiment, which runs the algorithm under a set of fixed parameters, is to show that the method recovers parameters effectively. The fixed parameters were generated through simulation with fixed Gaussian distributions with prior means 10,15, and 20 and prior variance parameters of 5. The first entries of each layer correspond to the noise block with fixed means at 5, 10 and 15. The means are: $\mu_{X,q} = (5, 11.98, 11.55, 10.39)$, $\mu_{Y,q} = (10, 16.86, 16.49, 14.81)$, $\mu_{Z,q} = (15, 16.69, 21.25, 21.08)$. The variances are $\Sigma_{X,q} = (7.88, 13.11, 0.31, 1.16)$, $\Sigma_{Y,q} = (7.32, 7.67, 4.89, 1.03)$, $\Sigma_{Z,q} = (6.69, 4.15, 0.06, 4.36)$. The correlations are $\rho_q = (0.00, 0.40, 0.15, 0.34)$, and the true group sizes are 76 nodes for the first block (NB), 97 for the second, 93 for the third, and 34 for the fourth.

Results

We generated 100 networks following these exact specifications and ran SBANM on all of them. In Figure 5 in the main text, each boxplot comprises a set of 100 estimates for each parameter values. The first row shows those for the first layer (written as \mathbf{X}), the second \mathbf{Y} , the third \mathbf{Z} , and the fourth for correlations between the three layers. The red band shows the true parameter values as listed above.

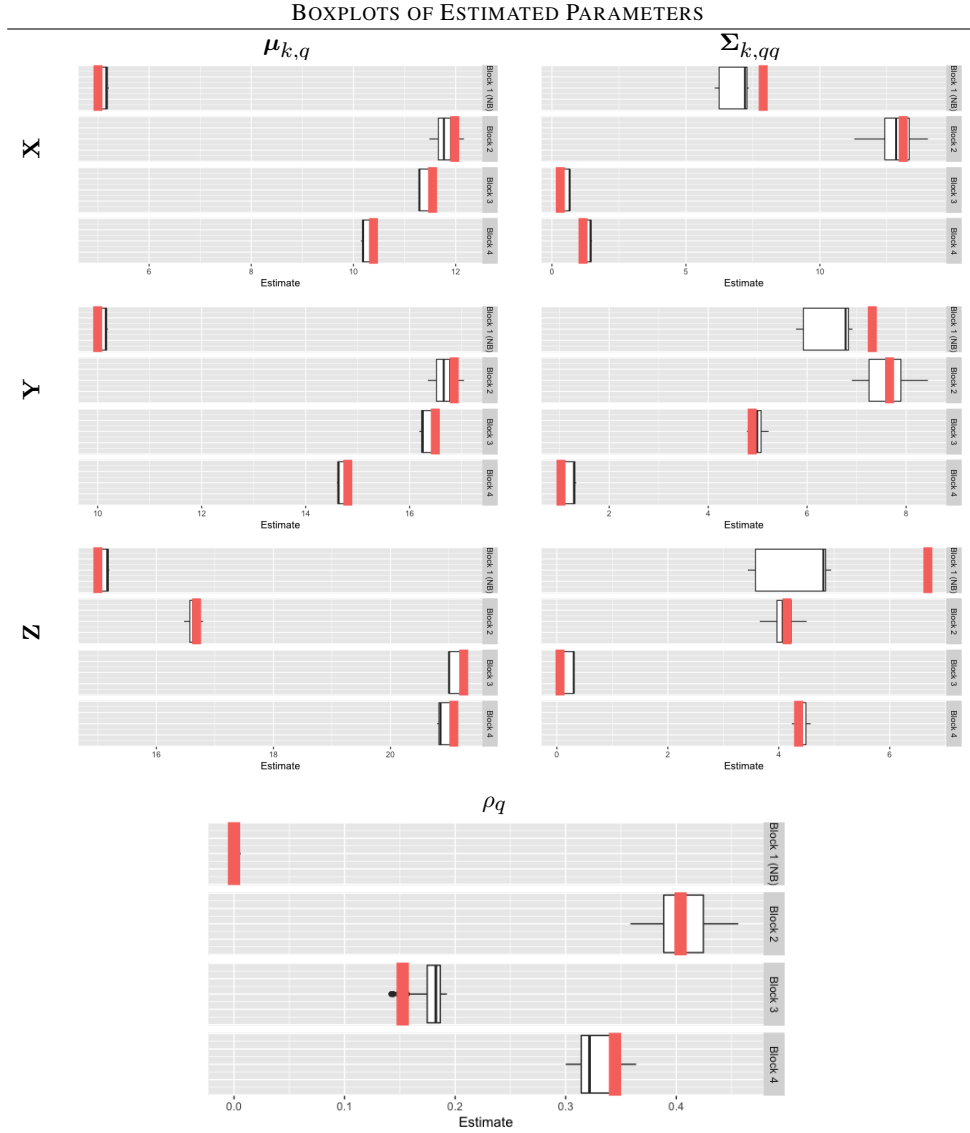


Fig 5: Boxplots for repeated estimates of simulations (second type). We ran the algorithm applied to 100 randomly generated networks with the same ground truth parameters and fixed sample sizes. Each boxplot represents the summary of 100 individual estimates corresponding to 100 runs. The red bands represent the ground truth parameters for means, variances, and correlations.

F.3. ICL Assessment (Experiment 3)

Model selection in the SBM clustering context usually refers to selection of the number of a priori blocks before VEM estimation as it is the only ‘free’ parameter in the specification step of the algorithm. Existing approaches [26, 50, 52] consider the *integrated complete likelihood* (ICL) for assessing block model clustering performance. Matias et al. write the ICL for multilayer graphs in the following way (adapted to match the notation of this study)

$$(16) \quad ICL(Q) = \log f(\mathbf{X}, \mathbf{Z}) - \frac{1}{2}Q(Q-1)\log(n(K-1)) - \text{pen}(n, K, \Theta)$$

to translate the terminology, Θ corresponds to the total set of transition parameters in the SBM, where $\Theta := \Theta_{\text{Signal}} \cup \Theta_{\text{Noise}}$ [52]. The penalty parameter $\text{pen}(\cdot)$ is chosen dependent on the distributions of the networks; the ‘Gaussian homoscedastic’ case in Matias et al. is derived to be

$$\text{pen}(n, K, \Theta) = Q \cdot \log \left(\frac{n(n-1)K}{2} \right) + \frac{Q(Q-1)}{2}K \cdot \log \left(\frac{n(n-1)}{2} \right).$$

Though the authors made the assumptions that the variances are constant for all blocks, we assume that the models are similar enough to SBANM such that the evaluation criterion is applicable to our case. For this portion of the simulation experiment we fix n at 200 and the ground-truth Q at 5. However, we apply the method for a range of hypothesized block numbers \hat{Q} (as the *estimate* for number of blocks) from 2 to 7. Simulation results show that the usage of ICLs caps at $\hat{Q} = 5$, the correct ground truth value (Figure 6).

Results: We used a single instance of a trivariate network with 200 nodes from the simulations generated in the first experiment (Section F.1). ICLs for five runs of the algorithm were calculated. Each run presupposed a different selection of Q from 2 to 7. The ground-truth value of Q is 5 and Figure 6 showed that the ground-truth Q captured the highest ICL.

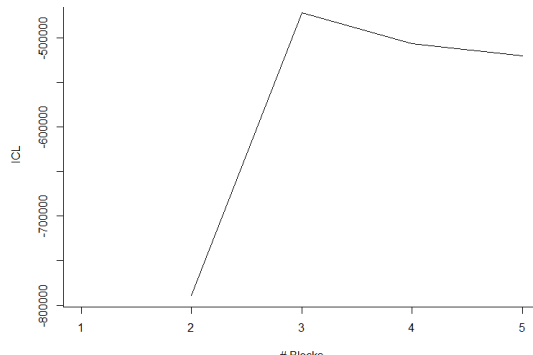


Fig 6: ICLs for simulation study for three-layer network of 200 nodes with a ground-truth Q of 5, which maps to the maximum ICL that was found by the method of estimation.

F.4. Large Network Simulations

For large-network simulations, single instances of networks with $n = 1000$ and 2000 are generated for $Q = 4$ and 5 . Results yielded exact recovery for memberships and within 5% errors for parameters.

APPENDIX G: DETAILS FOR ANALYSIS OF PNC DATA

G.1. PNC Preprocessing and Network Construction

The PNC has a well-represented sample with youth of mostly European American ancestry but include a substantial portion of African Americans. Roughly 21% met psychosis spectrum criteria and 4% reported threshold psychosis symptoms ([17]). We separately analyze the two age cohorts *youth* (with sample size 5136) and *early adult* (sample size 1863).

Response networks are constructed using a function that gauges similarity as well as positivity or negativity of responses. This distance function is similar to Hamming distance, but takes into account the direction of *positive* or *negative* agreement and is between -1 and 1. In a single graph-layer \mathbf{X}^k , a weight X_{ij}^k between two nodes is derived from indicators $h_{ij,u}^k$ across U questions (indexed by u) pertaining to a given set of conditions.

$$h_{ij,u}^k = \begin{cases} 1 & \text{if } i, j \text{ both answer "yes"} \\ -1 & \text{if } i, j \text{ both answer "no"} \\ 0 & \text{otherwise} \end{cases}$$

Each $h_{ij,u}^k$ between two subjects u, v is -1 if both answer no, 1 if both yes, otherwise 0. These values are then summed and divided by the total number of questions U :

$$r_{ij}^k = \frac{\sum_{u=1,\dots,U} h_{ij,u}^k}{U}.$$

The weight r_{ij}^k is 1 if two subjects both answer yes to everything and -1 if they answer no to everything. The weight r_{ij}^k is then transformed using a Fisher transformation to produce a value that approximates an observation in a normal distribution, in layer k : $X_{ij}^k = \text{Fisher}(r_{ij}^k)$.

G.1.1. Exploratory Histograms

We show exploratory histograms for the male early adult sample in the PNC data that serves as the primary sample for the analysis. Each edge (duplicates removed) show that each layer appears to be composed of a mixture of normal distributions.

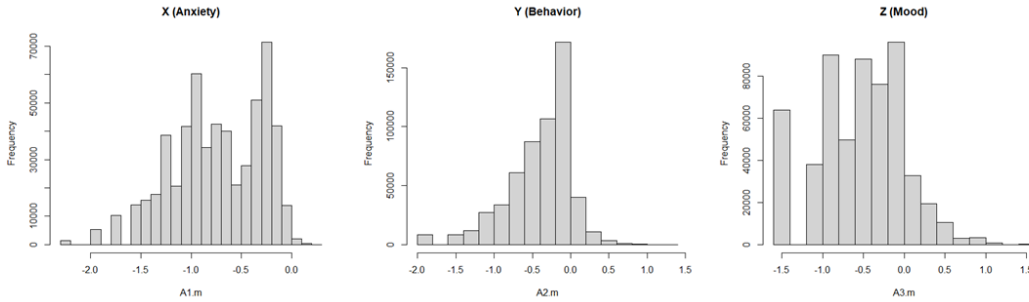


Fig 7: Histograms of the X, Y, Z layers representing the anxiety, behavior, and mood disorder layers.

G.2. Parameter Estimates and Demographic Characteristics

	block	n	ρ	μ_X	σ_X	μ_Y	σ_Y	μ_Z	σ_Z
1	NB	41	0.00	-0.63	0.31	0.02	0.39	-0.22	0.46
2	S_1	244	0.24	-0.23	0.15	-0.07	0.14	-0.02	0.48
3	S_2	471	0.27	-1.17	0.31	-0.76	0.43	-0.93	0.45

TABLE 3

Parameter estimates of SBANM in male early adults in PNC data. ρ represents the correlation, μ s represent the means, and σ s represent the variance.

Demographic characteristics among the separated blocks do not elucidate any major differences in sex, age, or race among the different clustered blocks. The *environmental impacts* variable, however, does show some major difference in the NB cluster, perhaps this shows that there could be some causal environmental effects into the psychosis-prone subjects. Unfortunately, we do not have more information on how exactly these environmental factors may play a role in this. Future research may investigate deeper into this relationship.

Demographic characteristics of the clustered subjects are shown in Table 4. Rates of patients who are African American, Hispanic, or female are roughly even across the board for most clusters for both youth and early adult under different Q specifications.

	Block	n	Age	Env.	Black	Hispanic	Female
1	NB	41	20	27	32%	5%	63%
2	S_1	244	20	-10	37%	7%	53%
3	S_2	471	20	-15	37%	6%	63%

TABLE 4

Demographic characteristics for SBANM in male early adults in PNC data. The variables represent age, environmental factors (Z-scores), percentage black, Demographic Characteristics of PNC Results. The columns represent respectively: age, environmental factors (Z-scores multiplied by 100), % African American, % Hispanic, and % Female

G.3. Additional Posthoc PNC Analyses

Hypothesis tests between different imputed blocks in PNC psychopathological networks (post-processed) and diagnostic categories showed significant differences between all the different clusters. In EA, though the diagnostic comparisons (right) are not all significantly different from each other, the signal (correlated) blocks are all significantly different from the noise block NB at the significance level of 0.05.

TABLE 5

Hypothesis tests for the clustered blocks in Youth subjects along two different criteria. In the first assessment (left), edges in the weighted network for each layer are treated as a i.i.d sample and compared to other edges using t-tests. In the second assessment, proportions of positive clinical diagnoses are tested across different imputed blocks. Recall that X represent the network of symptom response similarities for anxiety, Y for behavior, and Z for mood disorders.

EDGE COMPARISON FOR EA (3 GPS)				DIAGNOSIS COMPARISON FOR EA (3 GPS)				
B_q Comp.	X	Y	Z	%Anx	%Beh	%Mood	%TD	%Psy
$NB-S_1$	0.00 (**)	0.00 (**)	0.00 (**)	0.00 (**)	0.00 (**)	0.00 (**)	0.00 (**)	0.00 (**)
S_1-S_2	0.00 (**)	0.00 (**)	0.00 (**)	0.00 (**)	0.00 (**)	0.00 (**)	0.00	0.00 (**)
$NB-S_2$	0.00 (**)	0.00 (**)	0.00 (**)	0.00 (**)	0.03 (**)	0.00 (**)	0.00 (**)	0.00 (**)

APPENDIX H: ANALYSIS OF US CONGRESSIONAL VOTING

The focus of the study is on the PNC data. However, we also show the model’s generality by applying the method to political and human mobility data. We use SBANM to find latent patterns in longitudinal US congressional co-voting data to analyze the static as well as dynamic patterns in co-voting amongst US congressional districts, historically a fruitful domain of network analysis [22]. We also find clusters in longitudinal aggregations of bike-share networks, whose stations are represented by nodes. Analysis of zones amongst urban mobility services is elucidating for discovering latent patterns within human geography and demographic trends [19, 20, 32].

In the voteview data, each layer represents interactions among each congressional session. (\mathbf{X}, \mathbf{Y}) represents the 100th and 115th sessions of congress, respectively. n represents the number of congressional seats that are common to all three sessions (new or relabeled seats that were added since the first session are not included) Only two layers are used for this application of SBANM to the Divvy data, and (\mathbf{X}, \mathbf{Y}) in this case represents the normalized, aggregated trips between 2014-2016 and 2016-2018 respectively. The sample size $n = 547$ describes the total number of stations and each edge weight represents aggregate trips between stations.

We use congressional voting records from *Voteview* to uncover patterns in US congressional voting patterns that may yield more nuanced political groups than party labels (i.e. Democrat, Republican) over time. We use a similar pre-processing step as done for the PNC data to assign measures for co-voting similarities between seats in the US House of Representatives during the 100th, and 115th sessions. Voting similarities between representatives in Congress are represented as weighted edges between nodes (representing members). Each layer corresponds to a different congressional session. We apply the proposed model to data from the *Divvy* bikeshare system in Chicago called to show the ways that demarcating zones of bikeshare trips change across different years. Trip data for Divvy are publicly available on their respective websites [28].

The overarching motivation for this application is belied by the assumption that political parties change over time and do not necessarily capture the political “tribes” in the US House of Representatives in the past and the present. Prior work use co-voting patterns in the congress and senate in the United States to demonstrate applications of multilayer SBMs by representing district representatives (or senators) as nodes and their covoting similarities as edges [22, 83]. Though most congressional seats have fixed political parties that are representative of their political alignments, parties are assemblages of many constituents with issues that often fragment or congeal (ie polarize) over time. As such, it is useful to trace and segment the groups that either vote with each other persistently, or change drastically following some shift. Clustering different political ‘tribes’ by their similarities in voting is important for studying and forecasting patterns in US politics. It particular, it may be of interest to look for certain “swing” districts that yield more signal for political analysts to study, compared to the ambient levels of connectivity in politically non-contentious districts.

We procure voting data from *Voteview* [47]. We use data from all congressional line items from the 100th (1987-89), and 115th (2017-19) sessions, excluding consensus votes where all votes were ‘yes’ or ‘no’. These sessions sample distinct decadal political milieus in the United States across 30 years and serve as snapshots indicating long-term changes in the political inclinations of congressional districts. Though the number of these districts total 435 presently, differing seats often appear and vanish due to redistricting, and we use the seats that were common to both sessions. The resulting network size n is 393.

We use similarity measures similar to that which was applied to PNC survey data for voting records. Between two district seats, which are represented by nodes i and j , the total votes in

agreement (both yes or both no) are summed, then subtracted by the total disagreeing votes and divided by the total votes cast. We convert this correlation-like value, which is between -1 and 1, to a statistic that approximates to a normal distribution by applying the same Fisher transformation used in Section 2. Like in other studies [83], consensus votes that have either 100% “yes” or 100 % “no” are omitted.

We ran the algorithm over a range of values for estimated block numbers Q , as was done in Section 6.1. As the block sizes increase, the ICL also increases, until $Q := 3$ which is where it appears to attain a maximum. We display the clustering results for 3 blocks are

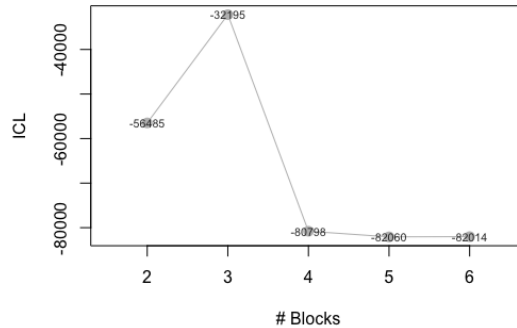


Fig 8: Block selection for US congressional voting data based on the method; 3 blocks yields the greatest ICL.

shown in Figure 8. In addition to the block sizes and estimated correlations, we show the average percentage of Republican party membership (%R) in the 100th and 115th sessions. The results show capture distinct shifts in party membership across the years: NB appears to capture the moderate niche of the congress.

MEMBERSHIPS, PARAMETERS, AND PARTY AFFILIATION						
Block	n	$\mu_{X,q}$	$\mu_{Y,q}$	ρ_q	%R(100th)	%R(115th) Notable People
NB	9	0.02	0.31	0.00	36	67 Nancy Pelosi (1)
S_1	233	0.71	0.36	0.09	4	50 Beto O’Rourke(2), Paul Ryan(2)
S_2	151	0.55	0.45	0.04	99	68 Dick Cheney(1), Liz Cheney(2)

TABLE 6

Clustering results for congressional voting data in the 100th and 115th sessions. In addition to the means and correlations of the (normalized) similarity networks, mean (Republican) party membership rates and notable people in each block are given.

Nine members in NB vote at the same rate with each other as with any other cluster; The interpretation of this block as *moderate* is supported by membership of *moderate Democrat* politicians such as Nancy Pelosi who occupied the seat during empirically verified by the fact that more than half of the block is Republicans in the 115th session. Moreover, NB yields the same rate as every other block votes at the same rate with a different block.

The two biggest political enclaves are large bipartisan *party* that is half Democrat and half Republican in 2015 but was almost entirely Democrat in 1987 (S_1), and another group that was almost entirely Republican in 1987 but only about 2/3 Republican in more recent times. The asymmetry in the blocks S_1 and S_2 is perhaps of note; one can view possibly S_2 as analogous to S_1 , but more likely the block is capturing an uneven relationship where there is no Democratic equivalent to the Republican block S_2 which shows entrenchment of voting ideology along geographical (district-wise) lines. These dynamics may be due to fundamental differences in voting patterns between the two parties. Results reveal the large drop-off in

the Democrats’ political dominance in the 100th session. Instead of capturing static (same-period) blocks, SBANM is able to capture some of the largest *differential* movements between the 1980s and 2015.

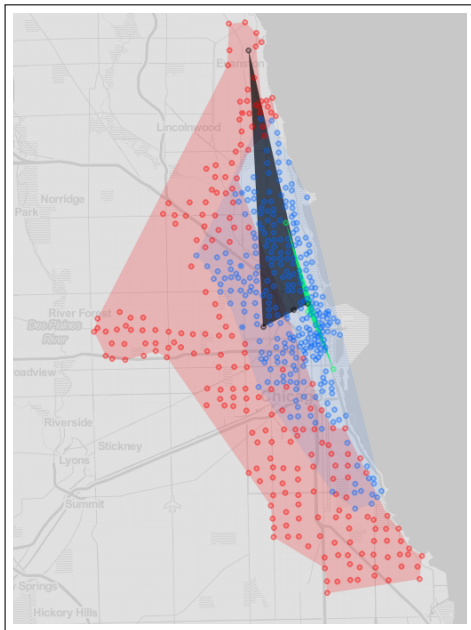
APPENDIX I: HUMAN MOBILITY DATA ANALYSIS

The SBANM method is applicable to human mobility patterns which is represented by bikeshare data. Bikeshare networks have been argued to trace the latent patterns within human mobility in urban systems [20]. He et al. [32] and others have modeled bikeshare stations as nodes and aggregate trips as edges [19], and then gathered conclusions about the patterns of human mobility within these bike-sharing constraints. In particular, prior work have analyzed differences in time-of-day patterns, functional differences (ie work-to-home and home-to-home trips), as well as long-term usage between neighborhoods. Carlen et al. have proposed a time-dependent SBM for (binary) paths between bikeshare stations [19]. We convert trip data from the public records of the *Divvy* bikeshare system into time-series networks where each edge represents trips and each node represents stations. We write these network time-series as $\{G_s\}_{1 \leq s \leq S}$, where S is the aggregate weekly time-points between January 2014 to June 2016, and $\{G_t\}_{1 \leq t \leq T}$ for T as the aggregate weekly time-points between July 2016 to December 2018, as was done a previous analysis of the *Divvy* system as conducted in He et al. [33]. New stations as well as stations that were removed during this time are omitted, such that the total number of stations ($n = 547$) is consistent across time.

We sum all of the edges across all time points for distinct time-periods S and T . The two graphs \mathbf{X} and \mathbf{Y} represent differential layers across two temporal regimes. We use the number of aggregated trips across each time-regime \mathbf{X} and \mathbf{Y} to represent edge-weights. The edge-weights are then transformed by dividing each value by the respective strengths (sum of weights) to procure a ratio between 0 and 1. The ratio is then converted into an approximately normal value by the *logit* transformation. Because of this transformation, mean values are negative and between -10 and -20. Estimated statistics (Figure 9) are reconverted using the inverse logit transform, then multiplied by the total graphwise sum-of-strengths, to convey a normalized mean rate of trips across stations within the same community.

Results show distinct geographical patterns (Figure 9). The red cluster is the largest (at 295 nodes) and represents a distinct baseline group for both time periods with activity that persist across time. The high inter-block correlation of .87 in this block suggests persistent trip interactions across time. The blue cluster represents a smaller (216 nodes) but a more *persistent* area of activity: it has higher means for both the first and second layers than that of S_1 for both time-regimes, and also has a high correlation rate. Because this area is closer to more affluent areas around the lake with more parklike amenities (such as the lakefront bike path), this block signifies zones with higher trip activity across both time periods.

Smaller groups NB and S_2 concentrate around the northern part of the city and have very different estimated means that signal drastic change in usage over time. Indeed, the green block S_2 has the highest first-layer mean μ_X but the lowest second layer mean μ_Y . That the correlation in this block across layers is zero furthermore suggests a disjointingly decreased usage over the two time periods. NB is represented by the grey-black cluster in the northwest part of the city and has the same parameters of ridership as riders traversing across different blocks; which offers an interpretation to the large, but not infeasible, distance between stations (members) in this block. These discovered clusters have interpretable results and suggests the viability of the method to human mobility data, after the appropriate transformations.



PARAMETER ESTIMATES					
		n	μ_X	μ_Y	ρ_q
●	NB	4	1.22	0.37	0
●	S_1	216	8.48	4.78	0.67
●	S_2	3	17.1	0.21	0.00
●	S_3	295	0.29	0.26	0.87

Fig 9: Communities found across 2 time-periods in the Divvy Bikeshare networks in Chicago, with associated (normalized) estimates for (normalized) mean rates of trips within the cluster in each time period, as well as correlations.